AGU PUBLICATIONS

Water Resources Research

RESEARCH ARTICLE
10.1002/2014WR016717

Key Points:
- The risk posed by chemical mixtures reaches a maximum at a critical distance
- Preferential channels can have beneficial or detrimental consequences on risk
- High-risk areas are the most reliable with Gaussian-like risk-pdfs

Correspondence to:
C. V. Henri,
christopher.henri@upc.edu

Citation:
Henri, C. V., D. Fernàndez-Garcia, and F. P. J. Barros (2015), Probabilistic human health risk assessment of degradation-related chemical mixtures in heterogeneous aquifers: Risk statistics, hot spots, and preferential channels, *Water Resour. Res.*, *51*, doi:10.1002/2014WR016717.

Received 2 DEC 2014
Accepted 9 MAY 2015
Accepted article online 13 MAY 2015

Probabilistic human health risk assessment of degradation-related chemical mixtures in heterogeneous aquifers: Risk statistics, hot spots, and preferential channels

Christopher V. Henri[1], Daniel Fernàndez-Garcia[1], and Felipe P. J. de Barros[2]

[1]Department of Geotechnical Engineering and Geosciences, Universitat Politècnica de Catalunya, Barcelona, Spain, [2]Sonny Astani Department of Civil and Environmental Engineering, University of Southern California, Los Angeles, California, USA

Abstract The increasing presence of toxic chemicals released in the subsurface has led to a rapid growth of social concerns and the need to develop and employ models that can predict the impact of groundwater contamination on human health risk under uncertainty. Monitored natural attenuation is a common remediation action in many contamination cases. However, natural attenuation can lead to the production of daughter species of distinct toxicity that may pose challenges in pollution management strategies. The actual threat that these contaminants pose to human health depends on the interplay between the complex structure of the geological media and the toxicity of each pollutant byproduct. This work addresses human health risk for chemical mixtures resulting from the sequential degradation of a contaminant (such as a chlorinated solvent) under uncertainty through high-resolution three-dimensional numerical simulations. We systematically investigate the interaction between aquifer heterogeneity, flow connectivity, contaminant injection model, and chemical toxicity in the probabilistic characterization of health risk. We illustrate how chemical-specific travel times control the regime of the expected risk and its corresponding uncertainties. Results indicate conditions where preferential flow paths can favor the reduction of the overall risk of the chemical mixture. The overall human risk response to aquifer connectivity is shown to be nontrivial for multispecies transport. This nontriviality is a result of the interaction between aquifer heterogeneity and chemical toxicity. To quantify the joint effect of connectivity and toxicity in health risk, we propose a toxicity-based Damköhler number. Furthermore, we provide a statistical characterization in terms of low-order moments and the probability density function of the individual and total risks.

1. Introduction

Monitored natural attenuation is an attractive cleanup technique commonly used to remediate organic and inorganic groundwater contaminants in field sites where biogeochemical conditions favor natural processes that degrade or immobilize harmful contaminants [*MacDonald*, 2000; *Kitanidis and McCarty*, 2012]. However, in some cases, before reaching a harmless chemical form, intermediate degradation products can constitute new noxious chemical compounds not necessarily less toxic than their parent product. In this situation, the original pollutants and their daughter products are susceptible to coexist in the aquifer forming an hazardous chemical mixture composed of products of different toxicity [*U.S. Environmental Protection Agency*, 2000]. This renders the quantification and interpretation of human health risk a nontrivial and challenging task.

The complexity associated with human health risk assessment for chemical mixtures stems from the interaction between aquifer heterogeneity, its uncertainty and the contaminant conditions (source characteristics, mixture composition, toxicity, and biochemical properties). The spatial heterogeneity of the hydrogeological properties will dictate the relative importance of the degradation products to the total human health risk. In this context, the variability of the hydraulic properties typically leads to preferential flow channels and low-permeability areas where contaminants can be temporarily trapped by rate-limited mass transfer [e.g., *Gomez-Hernandez and Wen*, 1998; *Zinn and Harvey*, 2003; *Bianchi et al*., 2011]. The formation of these fast flow channels is typically associated with the presence of well-connected, highly permeable geological bodies or structures that can concentrate flow and solute transport [e.g., *Knudby and Carrera*, 2005;

Fernàndez-Garcia et al., 2010; *Fiori and Jankovic*, 2012; *Renard and Allard*, 2013]. These geological features are difficult to model since characterization data are scarce and limited by financial budgets. Therefore, risk predictions associated with aquifer contamination are subject to uncertainty [e.g., *Rubin et al*., 1994; *Maxwell and Kastenberg*, 1999].

Incorporating hydrogeological uncertainty in human health predictions has been a topic of intense research in the past [e.g., *Andričević and Cvetković*, 1996; *Maxwell and Kastenberg*, 1999; *de Barros and Rubin*, 2008; *Cvetković and Molin*, 2012; *Rodak and Silliman*, 2011; *Andričević et al*., 2012; *Siirila and Maxwell*, 2012; *Atchley et al*., 2013; *de Barros and Fiori*, 2014]. Probabilistic risk models allow one to determine the likelihood of risk exceeding a given regulatory threshold value [*Tartakovsky*, 2007], to delineate the spatial distribution of a plume for monitoring adaptation or intensification [*James and Gorelick*, 1994; *Maxwell et al*., 1999; *Smalley et al*., 2000; *Maxwell et al*., 2007; *Fernàndez-Garcia et al*., 2012] and to better allocate characterization efforts to reduce the overall uncertainty of a given environmental performance metric [e.g., *de Barros et al*., 2009]. Most of the studies related to probabilistic risk analysis focused on the evaluation of human health risk posed by a single toxic compound.

Stochastic methods account for parametric uncertainty by considering aquifer parameters to be random space functions [*Rubin*, 2003]. In general, the computational effort associated with stochastic simulations of multicomponents reactive transport in three-dimensional heterogeneous aquifers has often limited risk analysis to simple scenarios. For example, a human health risk model related to multispecies groundwater contamination was reported by *Benekos et al*. [2007], who used a biochemical model to evaluate the human health risk response to a bioremediation scenario in a two-dimensional aquifer contaminated by chlorinated solvents. *Siirila et al*. [2014] investigated the total risk posed by the mobilization of metals from the leakage of CO_2. To reduce computational needs, the multispecies reactive-transport problem was tackled using a two-step approach that combined a simple one-dimensional geochemical model with fully three-dimensional transport simulations and sorption in local equilibrium. The role of kinetics was later on analyzed by *Atchley et al*. [2014], who used a simplified streamline approach. Despite the large body of the literature related to human health risk assessment, there are research needs to further understand the joint effect of degradation-related chemical mixtures and physical heterogeneity on human health risk.

Another factor that can influence risk predictions of chemical mixtures is the contaminant release behavior at the source zone. The importance of the source behavior is an aspect often disregarded in risk management. However, previous works demonstrated that a mass release proportional to local groundwater fluxes shows a strong and persistent impact on the contaminant spread, concentration amplitude and peak predictability [*Janković and Fiori*, 2010]. We hypothesize that this source behavior, together with the heterogeneous structure of the aquifer, will play a significant role in the health risk.

Within this context, this work focuses on improving our understanding of how heterogeneity (and connectivity) and the contaminant injection mode contributes to the creation of high-risk locations. To achieve our objective, we simulate high-resolution three-dimensional (3-D) flow and multispecies reactive transport within a stochastic framework. Human health risk is spatially characterized by lower-order statistical moments and empirical probability density functions for each individual chemical species and the total chemical mixture. We show that the total risk posed by a chemical mixture can increase to a maximum at a critical distance controlled by a modified, toxicity-based, Damköhler number that accounts for the joint effect of contaminant mean travel times, reaction kinetics, and chemical toxicity. Connectivity is shown to produce a nontrivial impact on risk measures, being potentially beneficial or detrimental depending on the proposed toxicity-based Damköhler number.

2. Problem Statement

This paper considers an aquifer contaminated by tetrachloroethylene (PCE), which is a common DNAPL product found in groundwater [*Fay and Mumtaz*, 1996]. PCE pure liquid is assumed to be already trapped (immobile) in the aquifer but slowly dissolving over time. This creates a long-term contamination plume downgradient. Under anaerobic conditions, chlorinated solvents dissolved in groundwater can undergo reductive dechlorination [*Skeen et al*., 1995; *Jain and Criddle*, 1995]. In such a case, PCE will be transformed into trichloroethylene (TCE), TCE will be degraded into *cis*-Dichloroethylene (DCE) (Dichloroethylene), DCE will react to produce vinyl chloride (VC) and, finally, VC will transform into a nontoxic compound, ethene.

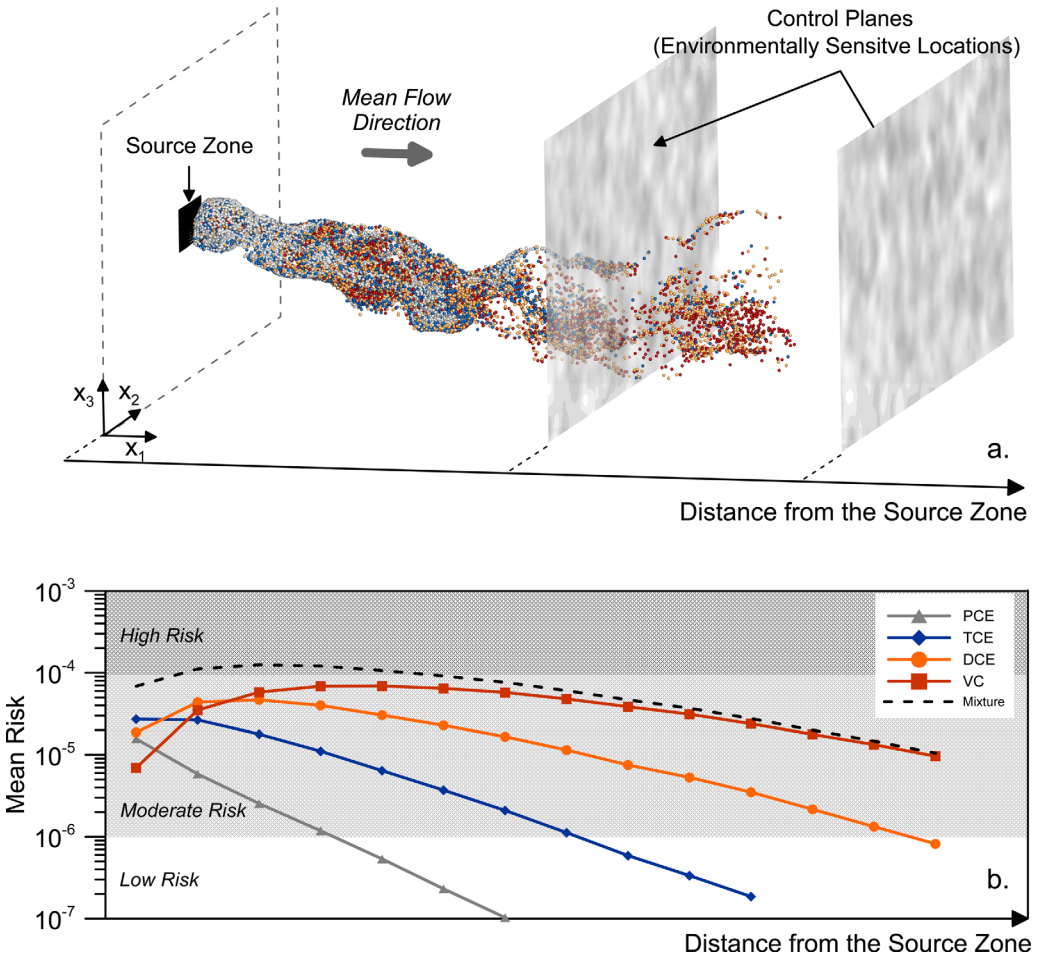

Figure 1. (a) Snapshot of a contaminants mixture plume (grey : PCE, blue: TCE, orange: DCE, red: VC) approaching control planes and transported in a 3-D heterogeneous hydraulic conductivity field. (b) Expected risk profile along the contaminated site.

This constitutes a sequential reaction of the form PCE → TCE → DCE → VC → ethene. The four chlorinated compounds can cause a potential risk on human health that we aim to quantify here. PCE, TCE, and DCE are categorized as probable human carcinogenic (e.g., limited evidence) by the *U.S. Environmental Protection Agency* [1997]. However, VC is categorized as a human carcinogen (sufficient human evidence for causal association between exposure and cancer) [*U.S. Environmental Protection Agency*, 1997]. Parent and daughter species of different toxicity temporarily coexist in a chemical mixture. A 3-D snapshot of the contaminant and its daughter products is shown in Figure 1a. An illustrative example of the spatial evolution of the human health risk for each chlorinated solvent can be seen in Figure 1b. Interestingly, a high-risk zone can be expected far from the contaminant source.

Given that a significant fraction of DNAPL mass is likely to remain in aquifers even after a given remediation treatment, *Soga et al.* [2004] proposed to consider what is an acceptable contamination level not based on the amount of DNAPL mass removed from the site but by measurements of dissolved concentrations downgradient. They called this methodology *the mass flux approach*. Here following this strategy, the estimation of human health risk is strictly based on integrated concentration breakthrough curves, which are obtained at *x*-control planes perpendicular to the mean flow direction.

2.1. Human Health Risk Model

In this work, we will focus on quantifying cancer risk due to chronic exposure to chlorinated solvents released in a spatially heterogeneous aquifer. The route of exposure is assumed to be only direct ingestion. Following the human health risk assessment guidance [*U.S. Environmental Protection Agency*, 1989], carcinogenic health risk can be evaluated by a Poisson model for individual cancer occurrence, where $R_i(x)$ is the

Table 1. Risk Parameters

Parameter	Value			
Ingestion rate, *IR* (L/d)	1.4			
Body weight, *BW* (kg)	70.0			
Exposure duration, *ED* (year)	30.0			
Exposure frequency, *EF* (d/yr)	350.0			
Average time of the expected lifetime, *AT* (day)	25,550.0			
	PCE	TCE	DCE	VC
Cancer potency factor, CPF_i (kg d/mg)	0.0021	0.011	0.6	1.5
Maximum contaminant level, MCL_i (μg/L)	5.0	5.0	7.0	2.0

incremental lifetime cancer risk (ILCR) to a contaminant *i* at a given longitudinal position *x* where the control plane is located. The ILCR can be formally written as:

$$R_i(x) = 1 - \exp\left[-ADD_i(x) \times CPF_i\right], \tag{1}$$

where CPF_i (kg d/mg) is the metabolized cancer potency factor related to the carcinogenic contaminant *i*, and ADD_i (mg/(kg d)) is the average daily dose of contaminant *i*. Here we will only consider human exposure by direct ingestion so that:

$$ADD_i(x) = \bar{c}_i(x)\left[\frac{IR}{BW}\right]\frac{ED \times EF}{AT}, \tag{2}$$

where *IR* is the ingestion rate of water (L/d), *BW* is the body weight (kg), *AT* is the expected lifetime (day), *ED* is the exposure duration (year), and *EF* is the daily exposure frequency (d/yr). These parameters are assumed constant and defined in Table 1. The key component in the evaluation of the average daily dose is $\bar{c}_i$ (mg/L), which is the critical (flux-averaged) concentration of the pollutant *i* at an environmentally sensitive location *x*. This parameter $\bar{c}_i$ can be seen as the maximum running averaged concentration of the concentration breakthrough curve obtained at the control plane (CP) over the exposure duration *ED* [*Maxwell and Kastenberg*, 1999]. Note that, by convention, lowercase and uppercase concentrations will, respectively, denote flux-averaged and resident concentrations throughout this work [*Parker and Van Genuchten*, 1984]. The maximum running averaged concentration is mathematically expressed by:

$$\bar{c}_i(x) = \max_{t>0}\left\{\frac{1}{ED}\int_t^{t+ED} c_i(\tau; x)\, d\tau\right\}, \tag{3}$$

where $c_i(\tau; x)$ is the flux-averaged concentration defined as the ratio of the mass discharge to the volumetric water flux at a control plane location *x*. We note that flux-averaged concentrations have been widely used in previous human health risk analysis [*Andričević and Cvetković*, 1996; *de Barros and Rubin*, 2008].

Another important metric is the total risk associated with the chemical mixture (e.g., PCE, TCE, DCE, and VC). The total risk R_T defines the effective threat posed by the exposure to a chemical mixture. When contaminant concentrations are low enough (lower than 300 ppm), the total risk can be satisfactorily determined by the sum of individual risks [*Speek*, 1981],

$$R_T(x) = \sum_{i=1}^{4} R_i(x). \tag{4}$$

Stake-holders and regulators sometimes prefer to determine aquifer remediation goals in terms of maximum contaminant levels (MCLs), defined by the United States Environmental Protection Agency as the legal threshold limit of a contaminant concentration allowed in public water systems. To analyze this scenario, we also investigate the spatiotemporal behavior of the probability of exceedance of MCLs associated to each chemical species *i*,

$$\xi_{c_i}(x, t) = \text{Prob}[c_i(t; x) > MCL_i]. \tag{5}$$

From a practical perspective, an important issue for risk assessors is the characterization of *hot spots* and *hot moments*. A hot spot is typically defined as an area of elevated risk [*Dilley et al*., 2005]. The level at which the risk is considered elevated is usually determined by stakeholders and end-users during the risk assessment and decision making process. This concept will be used here to qualitatively highlight an area of maximum risk. When dealing with the ILCR, which is an integrated measure over time that only depends on *x* (see equation (3)), the corresponding hot spot will refer to the *x*-interval with maximum ILCR values. Instead, when dealing with the probability of exceedance of MCLs, the hot spot will indicate the spatial window for which $\xi_{c_i}(x, t)$ reaches a relatively large value at any given time. The temporal persistence of these high

values is denoted as the *hot moment*, which is only an intrinsic property of $\xi_{c_i}(x,t)$. Importantly, results will show that the location of critical hot spots can drastically change with the risk metric employed (probability of exceedance of MCLs or increased lifetime cancer risk).

2.2. Flow and Transport Model

In order to determine $\bar{c}_i$ (3), we need to simulate flow and reactive transport. In this work, we consider a 3-D confined aquifer. The Cartesian coordinate system is given by $\mathbf{x} = (x, y, z)$. The domain is a rectangular prism with length $L_x = 1600$ m, width $L_y = 800$ m, and thickness $L_z = 400$ m. The aquifer has constant head boundaries at $x = 0$ m and $x = 1600$ m and no-flow conditions at the remaining boundaries. Groundwater flow is at steady state and driven by a mean horizontal hydraulic gradient given by $J = 0.07$ and oriented in the x direction. Groundwater fluxes are described by Darcy's law through,

$$\mathbf{q}(\mathbf{x}) = -K(\mathbf{x})\nabla h(\mathbf{x}), \tag{6}$$

where $\mathbf{q}$ (m d^{-1}) is the specific discharge, h (m) is the hydraulic head, and K (m d^{-1}) is the hydraulic conductivity at the $\mathbf{x}$ location. The hydraulic conductivity is assumed locally isotropic but spatially heterogeneous. In this case, the groundwater flow equation is:

$$\nabla \cdot [K(\mathbf{x})\nabla h(\mathbf{x})] = 0. \tag{7}$$

The reductive dechlorination of PCE due to biodegradation can be approximated by a sequential first-order reaction kinetic model [e.g., *Clement*, 2001; *Burnell et al*., 2014]. This model assumes that contaminant concentrations are relatively low (below the Michaelis half-saturation constant) [*Cunningham and Mendoza-Sanchez*, 2006]. Reactive transport of PCE and its degradation products can be described by the following system of partial differential equations:

$$\phi \mathcal{R}_i \frac{\partial C_i}{\partial t} - \nabla \cdot (\phi \mathbf{D} \nabla C_i) + \nabla \cdot (\mathbf{q} C_i) = y_i k_{i-1} \phi C_{i-1} - k_i \phi C_i + s(\mathbf{x}, t)\delta_{i1}, \ \forall i = 1, \ldots, 4, \tag{8}$$

where ϕ is the porosity, $\mathbf{D}$ (m^2 d^{-1}) is the hydrodynamic dispersion tensor, and δ_{i1} is the Kronecker delta function. The dispersion tensor $\mathbf{D}$ is oriented in the direction of flow with principal components determined by $D_L = \alpha_L v$, $D_{TH} = \alpha_{TH} v$, and $D_{TV} = \alpha_{TV} v$. Here v (m/d) is the velocity of groundwater, α_L (m) is the longitudinal dispersivity, α_{TH} (m) is the horizontal transverse dispersivity, and α_{TV} is the vertical transverse dispersivity (m). Dispersivity coefficients are assumed constants for all species and molecular diffusion is neglected. For each species i, $\mathcal{R}_i$ is the retardation factor, C_i (g m^{-3}) is the resident concentration in the liquid phase, k_i (day^{-1}) is the first-order contaminant degradation rate constant, and y_i (g g^{-1}) is the effective yield coefficient for any reactant or product pair. These coefficients are defined as the ratio of mass of species i generated to the amount of mass of species $i-1$ consumed. Sorption reactions are assumed in local equilibrium and follow a linear sorption isotherm [*Roberts et al*., 1986]. Transport equations consider that no biodegradation occurs in the sorbed phase. Nevertheless, we note that other scenarios can be simulated by properly redefining the degradation rates.

The aquifer is considered to be initially clean (zero concentration of PCE and its degradation products at time $t = 0$) but subject to a PCE time-dependent source dissolution rate $s(\mathbf{x}, t)$ (mass per unit volume and time). This term represents the mass of dissolved PCE leaving the source zone through a rectangular area A_s. This area is centered within a vertical plane located at $x_{inj} = 200$ m and has a size of 96×48 m^2 (see Figure 1).

2.3. Source Mass Release Model

Several mass-depletion models have been proposed in the literature to effectively represent DNAPL dissolution at a contaminated site. Among them, we employ the power law empirical model proposed by *Rao et al*. [2001] and *Parker and Park* [2004], which describes the relationship between the flux concentrations of the dissolved DNAPL leaving the source zone and the mass of DNAPL remaining in the source zone as:

$$\frac{c_s(t)}{c_0} = \left(\frac{m(t)}{m_0}\right)^{\Gamma}, \tag{9}$$

where c_s is the averaged flux concentration of the dissolved DNAPL chemical (PCE) leaving the source zone, c_0 is the corresponding initial concentration, and Γ is the mass-depletion constant that accounts for

changes in interfacial surface area as the source mass diminishes. Typically, Γ is larger than 1 for contaminated sites with finger-dominated residual DNAPL, and smaller than 1 for sites with prominence of DNAPL pools and lenses [*Parker and Park*, 2004]. This is due to the fact that finger-dominated sources generally exhibit higher initial mass transfer coefficients per unit mass than lens-dominated systems. Substituting (9) into the mass balance equation expressed at the source zone, the flux concentration of PCE leaving the source zone can be determined from *Parker and Park* [2004] as:

$$c_s(t)=\frac{c_0}{m_0^{\Gamma}}\left\{\frac{-Q_s c_0}{\lambda_s m_0^{\Gamma}}+\left(m_0^{1-\Gamma}+\frac{Q_s c_0}{\lambda_s m_0^{\Gamma}}\right)e^{(\Gamma-1)\lambda_s t}\right\}^{\frac{\Gamma}{1-\Gamma}}, \tag{10}$$

where m_0 is the initial mass of DNAPL at the source zone, Q_s is the groundwater volumetric discharge rate passing through the source zone, and λ_s is the first-order degradation constant of PCE at the source zone. Based on this, the time-dependent source dissolution rate $s(\mathbf{x},t)$ can be written as:

$$s(\mathbf{x},t)=q_s c_s(t)\,\delta(x-x_{inj})\Omega(\mathbf{x}\in A_s), \tag{11}$$

where $q_s=Q_s/A_s$, Q_s is the total flow passing through A_s, and $\Omega(\mathbf{x}\in A_s)$ is an indicator function that is equal to one when $\mathbf{x}\in A_s$ and zero otherwise.

It is common in modeling studies to distribute the total discharge mass of DNAPL leaving the source zone homogeneously in the outlet source area. However, spatial variations in the aquifer hydraulic properties may suggest more complicated source behaviors [*Parker and Van Genuchten*, 1984; *Fure et al*., 2006]. Two scenarios will then be considered in this work: a *classical mass injection mode* (CIM) related to a homogeneous distribution and a *flux-weighted injection mode* (FWIM) related to a flux-weighted distribution of PCE at the outlet source area.

3. Methodology

A stochastic framework is used to account for the uncertainty in the hydraulic conductivity field, which is described as a random space function. In this work, health risk statistics are characterized through numerical Monte Carlo simulations. Analytical stochastic approaches based on perturbation theory are available in the literature to estimate human health risk associated with individual species [e.g., *Andričević and Cvetković*, 1996; *de Barros and Rubin*, 2008; *de Barros and Fiori*, 2014] but few works have assessed the risk posed by chemical mixtures in highly heterogeneous 3-D aquifers. For this work, the state variables (i.e., ILCR) are characterized by their statistical moments and empirical probability density functions (*pdf*s). Monte Carlo simulations consist of four sequential steps: (1) stochastic generation of equiprobable hydraulic conductivity fields; (2) solve the flow problem associated to each hydraulic conductivity field; (3) solve the reactive-transport problem for each flow field; and (4) estimate the corresponding ILCR at different control planes.

Table 2. Physical Parameters Adopted for Simulating Serial Reaction Transport in a 3-D Heterogeneous Flow System

Parameter	Value
Flow Problem	
Average hydraulic gradient	0.07
Longitudinal dispersivity, α_L (m)	0.4
Transversal dispersivity in the horizontal plane, α_{TH} (m)	0.04
Transversal dispersivity in the vertical plane, α_{TV} (m)	0.01
Porosity, ϕ	0.3
Heterogeneous Field	
Variogram type	Gaussian
Mean of Y ($Y=\ln K$) (m^2/d)	0.0
Variance of Y	1.0 and 4.0
Integral scales, $\lambda_x=\lambda_y=\lambda_z$ (m)	14.18
Domain Discretization	
Number of cells in x direction, n_x	400
Number of cells in y direction, n_y	220
Number of cells in z direction, n_z	100
Cell dimension, $\Delta_x\times\Delta_y\times\Delta_z$ (m × m × m)	4.0 × 4.0 × 4.0

The log conductivity field, denoted as $Y(\mathbf{x})=\ln K(\mathbf{x})$, is considered to follow a multi-Gaussian random space function model characterized by an isotropic Gaussian covariance function with zero mean and an integral scale λ of 14.18 m. Two levels of heterogeneity of $Y(\mathbf{x})$ were explored: $\sigma_Y^2=1$ and $\sigma_Y^2=4$. These values were chosen to represent a mild and a highly heterogeneous aquifer scenario. The geostatistical parameters of the $Y(\mathbf{x})$ random field are summarized in Table 2. The domain is discretized into 400 × 200 × 100 squared cells that form an 8 million cell problem. The Monte Carlo simulations considered 500 equiprobable realizations of the $Y(\mathbf{x})$ random field. The Monte Carlo convergence was controlled by analyzing

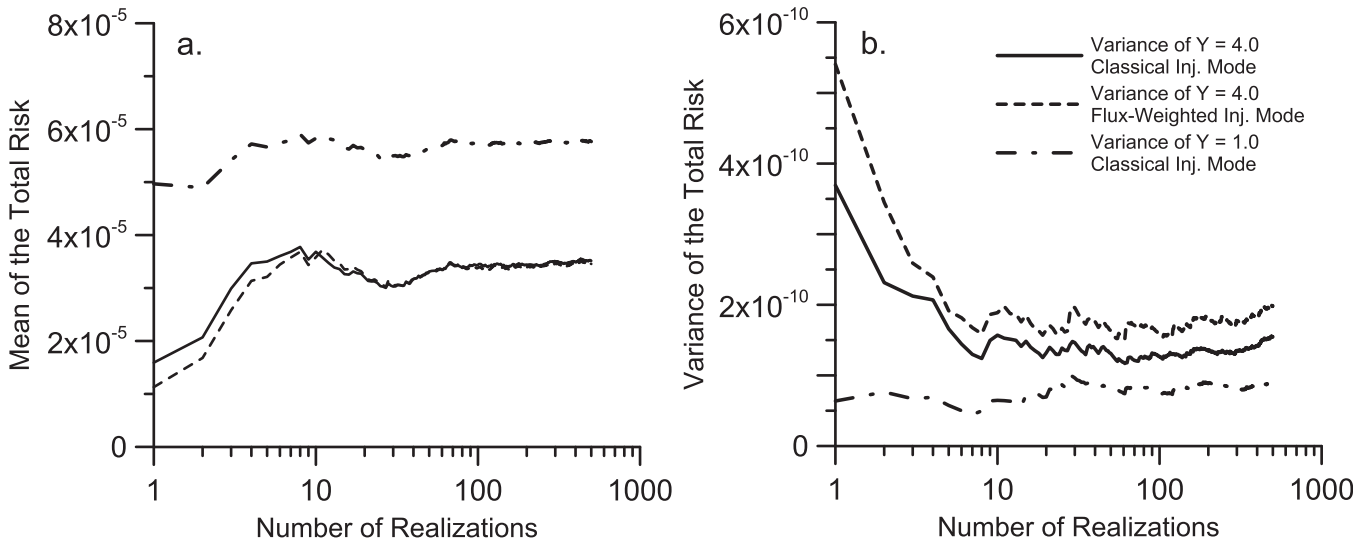

Figure 2. (a) Monte Carlo convergence of the total mean increased lifetime cancer risk and (b) its variance as a function of the number of realizations obtained at the control plane $\zeta = 24.7$ for the three different scenarios.

the stabilization of the mean and variance of total risk. Figure 2 shows a satisfactory stabilization of the two first statistical moments after 100 realizations.

For each $Y(\mathbf{x})$ realization, the groundwater flow equation (7) was first solved by means of the well-known finite difference code, MODFLOW [*Harbaugh et al.*, 2000]. The multispecies reactive-transport problem formed by PCE, TCE, DCE, and VC was then simulated using the random walk particle tracking (RWPT) methodology using the RW3D code [*Fernàndez-Garcia et al.*, 2005]. This code has been recently adapted to efficiently simulate first-order network reaction systems [*Henri and Fernàndez-Garcia*, 2014]. RWPT simulates solute transport by injecting a large number of mass particles into the system. Particles move by following the velocity field obtained from the solution of the flow equation to simulate advection and adds a random displacement to simulate dispersion [e.g., *Salamon et al.*, 2006; *Boso et al.*, 2012]. First-order network reactions are simulated by changing the species state assigned to each particle based on transition probabilities that depend on the biochemical properties of the species. The particle-tracking code can efficiently model such multispecies systems in heterogeneous conditions and at high resolution. We refer to *Henri and Fernàndez-Garcia* [2014] for further numerical details. Transport parameters are characterized by a constant porosity (ϕ=0.3), a longitudinal dispersivity of 0.4 m, a horizontal transverse dispersivity of 0.04 m, and a vertical transverse dispersivity of 0.01 m (see Table 2). Based on the review of field dispersion data by *Gelhar et al.* [1992], these grid-cell values of dispersivity were estimated as $\alpha_L \approx 0.1\Delta x$, and $\alpha_L/\alpha_{TH} \approx 10$ to account for subgrid heterogeneity. Biodegradation rates (k_i) are assumed constant in space and were chosen according to the range of possible first-order rate constants observed and summarized by the *U.S. Environmental Protection Agency* [1999]. The retardation factors were chosen according to the expected differences in mobility between the different chlorinated chemicals [*Lu et al.*, 2011]. The adopted reaction parameters are depicted in Table 3.

A large number of PCE particles (n=10^5) were instantaneously released at $\mathbf{x} \in A_s$. In terms of the correlation structure, the size of the source area A_s is $6.8\lambda \times 3.4\lambda$, which is similar to reported field conditions at the Borden and Cape Cod sites [e.g., *Mackay et al.*, 1986; *LeBlanc et al.*, 1991]. The first arrival time of particles passing through a set of control planes was recorded during the simulation, from which cumulative breakthrough curves were estimated, $c_i^h(t;x)$. The concentrations of all species $c_i(t;x)$ produced by a time-dependent injection were then estimated using the principle of superposition, which states that:

$$c_i(t;x) = \int_0^t c_s(\tau) c_i^\delta(t-\tau;x)\, d\tau, \qquad (12)$$

Table 3. Reaction Parameters

	Value			
Parameter	PCE	TCE	DCE	VC
First-order decay, k_i (day^{-1})	0.0025	0.002	0.0015	0.001
Yield coefficient, y_i (g g^{-1})		0.79	0.74	0.64
Retardation factor, $\mathcal{R}_i$	7.1	2.9	2.8	1.4

Table 4. Source Zone Mass Transfer Parameters

Parameter	Value
Power law, Γ	2.0
Initial concentration, C_0 (g/m^3)	0.1
Initial mass, M_0 (kg)	300.0
Source first-order decay rate, λ_S (day^{-1})	5×10^{-4}

where $c_i^{\delta}(\tau;x)$ is the Dirac-input solution (instantaneous injection) of the concentrations associated with the ith species. By discretizing the source term in step functions, $c_s(t)=c_{s,0}H(t)+\sum_{j=1}\Delta c_{s,j}H(t-t_j)$, being $H(t)$ the heaviside step function and $\Delta c_{s,j}=c_{s,j}-c_{s,j-1}$, equation (12) can be written as:

$$c_i(t;x)=c_{s,0}c_i^h(t;x)+\sum_{j=1}^{t_j<t}\Delta c_{s,j}c_i^h(t-t_j;x), \tag{13}$$

where $c_i^h(t;x)$ is the cumulative breakthrough curve of the ith species obtained from a unitary mass source. The mass-depletion model parameters are summarized in Table 4.

The distribution of particles in the source area followed the two injection modes previously discussed (i.e., CIM and FWIM). The CIM injection mode injected the particles uniformly within the source area and the FWIM injection mode distributed the particles proportional to local cell fluxes.

4. Statistical Description of Risk

Computational results are organized as it follows: section 4.1 presents the probability of exceedance of the maximum contaminant levels (MCLs). Then, section 4.2 offers the statistical description of the total ILCR. The statistical description of the total ILCR is based on low-order statistics (ensemble mean and coefficient

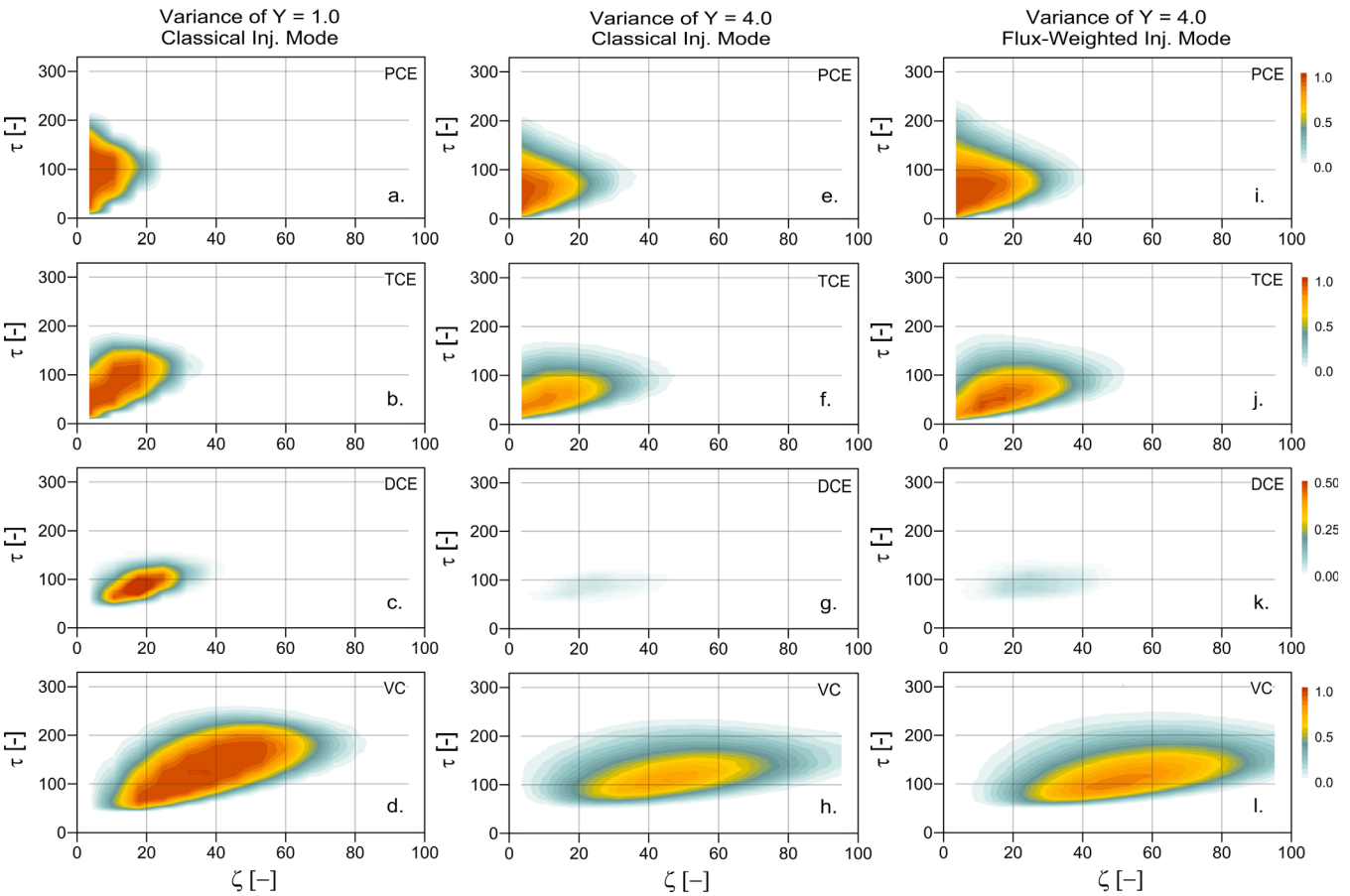

Figure 3. (left) Risks of exceedance of the MCLs as a function of the normalized time τ and the normalized distance ζ related to a variance of Y of 1.0 (frames a–d), (middle) a variance of Y of 4.0 for a classical injection mode (frames e–h), and (right) a variance of Y of 4.0 for a flux-weighted injection mode (frames i–l).

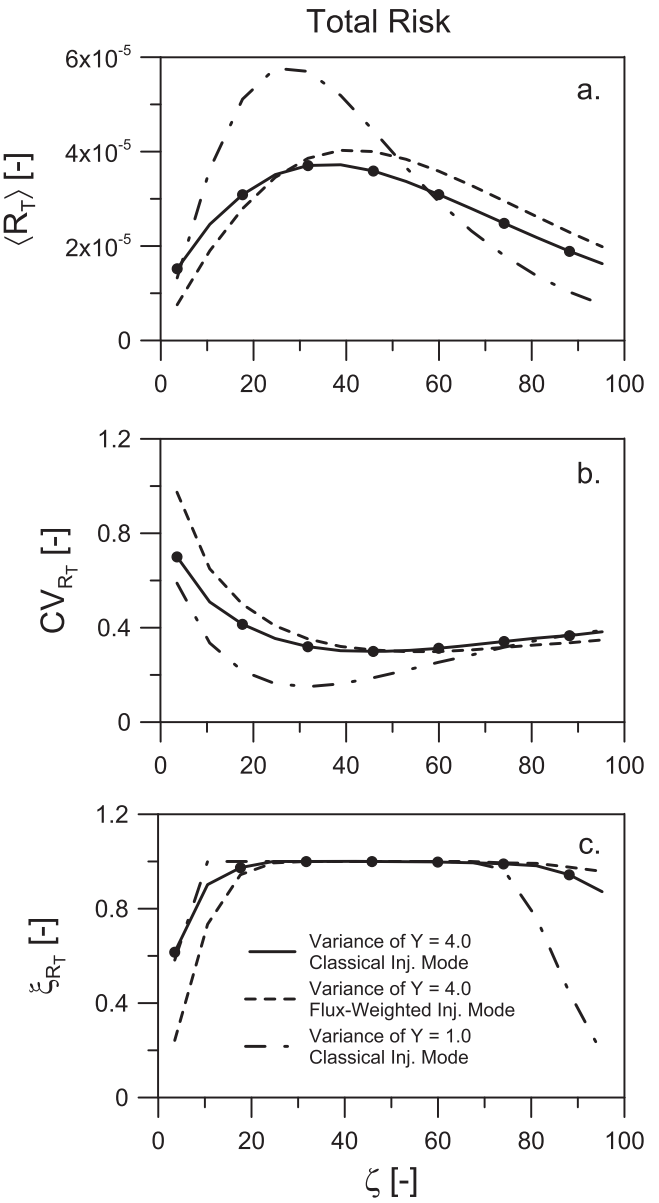

Figure 4. (a) Longitudinal profile of the expected mean of the total increased lifetime cancer risk, (b) its coefficient of variation, and (c) its reliability function.

of variation) as well as on the full characterization of the *pdf*. The mean of the total ILCR, denoted here as $\langle R_T(x) \rangle$, is a measure of the expected threat to the exposed population. Instead, the coefficient of variation of the total ILCR, given by $CV_{R_T}(x) = \sigma_{R_T}(x) / \langle R_T(x) \rangle$, where σ_{R_T} is the standard deviation of the total ILCR, provides a measure of the degree of uncertainty in risk predictions.

We also analyzed the so-called survival or reliability function of the total risk (ξ_{R_T}), i.e., the probability of exceedance of a given threshold R^*, denoted as $\xi_{R_T}(x) = \text{Prob}[R_T(x) > R^*]$. This function identifies the area at which the risk persists beyond a specified threshold normally defined by regulators. Typical values range between 10^{-4} and 10^{-6}. For the purpose of illustration, we set $R^* = 10^{-5}$. In the following, results are presented in dimensionless variables. The longitudinal distance from the injection $(x - x_{inj})$ is normalized by the integral scale λ, i.e.,

$$\zeta = \frac{x - x_{inj}}{\lambda},$$

and the time elapsed from the beginning of the contamination is normalized by the expected time needed to travel an integral scale, i.e.,

$$\tau = \frac{t K_G J}{\lambda \phi},$$

where K_G is the geometric mean of the hydraulic conductivity, and J the hydraulic gradient.

4.1. Probability of Exceedance of MCLs

The visualization tool proposed here to analyze probabilities of exceedance of MCLs, i.e., $\xi_{c_i}(x,t) = \text{Prob}[c_i(t;x) > \text{MCL}_i]$, provides a useful information on the temporal and the spatial distribution of risk posed by the contamination. This graphical tool allows decision makers to identify the spatial range in which high values of $\xi_{c_i}(x,t)$ are predicted (*hot spots*) and the temporal persistence of these high values (*hot moments*). Figure 3 displays the spatiotemporal evolution of $\xi_{c_i}(\mathbf{x},t)$ for each chemical compound as a function of σ_Y^2 and the injection mode. Results show that the probability of exceedance is highly sensitive to the species of concern. The area limited by nonnegligible probabilities of exceedance increases with decreasing MCL. Thus, the degradation product VC with the lowest MCL produces an extended region of low risk reliability both in space and time. The opposite occurs for the degradation product DCE with the highest MCL. An increase in σ_Y^2 leads to the dilution and spreading of the probabilities of exceedance in all contaminant products. Consequently, the threat is smaller in magnitude but occupies a larger

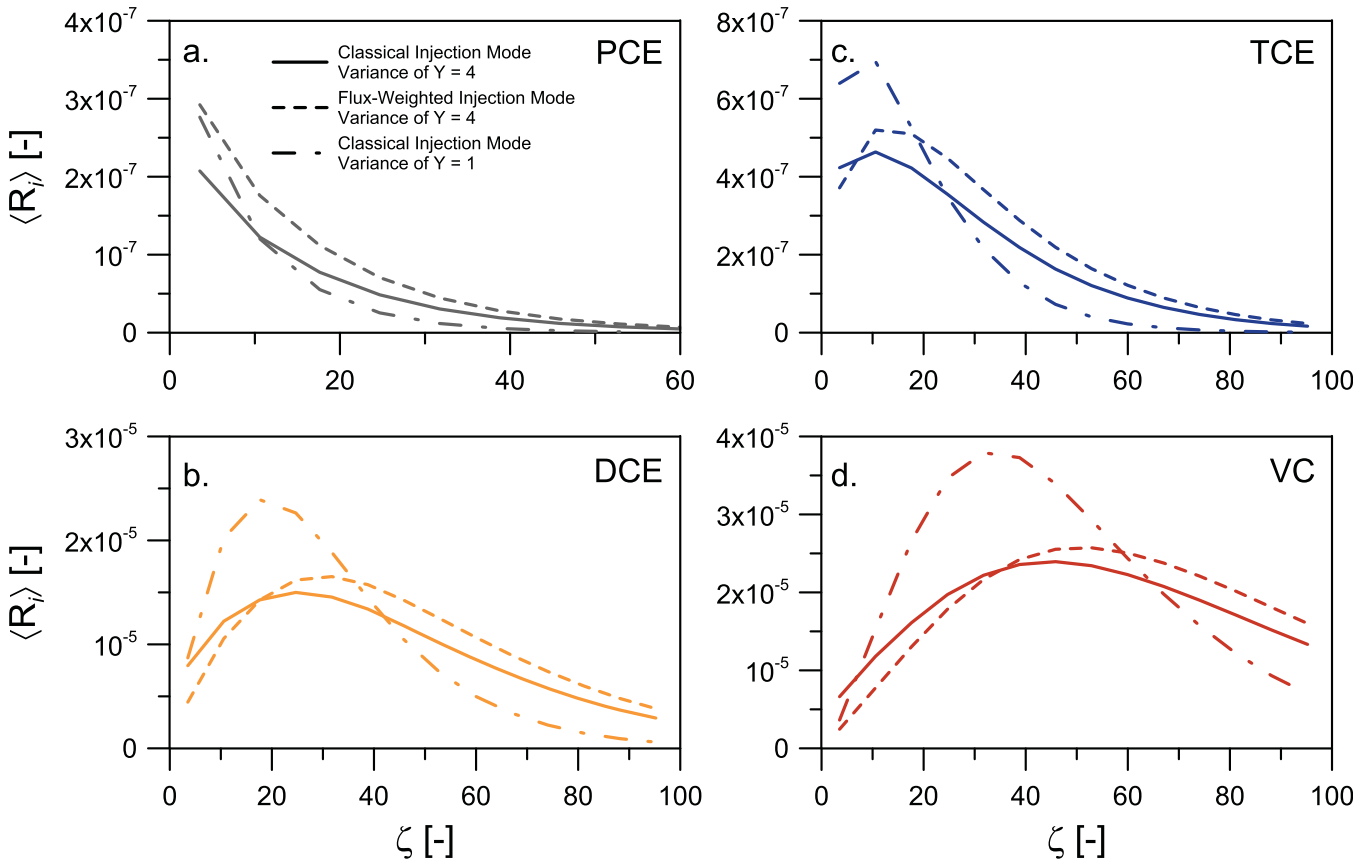

Figure 5. Influence of the variance of Y and of the injection mode on the longitudinal distribution of the individual mean risk, for the compounds (a) PCE (grey) and (b) TCE (blue), and the compounds (c) DCE (orange) and (d) VC (red). Distances from the injection are normalized by the integral scale as $\zeta=(x_{cp}-x_{inj})/\lambda$.

spatiotemporal region. Nevertheless, the spreading mostly takes place in the spatial dimension ζ. Remarkably, concentrations can exceed the MCLs during a larger period of time with smaller σ_Y^2 (compare frames a–d with e–h).

The type of injection has substantial consequences on the spatiotemporal evolution of $\xi_{c_i}(\mathbf{x},t)$. A flux-weighted injection can drastically increase the magnitude and area occupied by the nonnegligible probability of exceedance. This seems to suggest that the dilution of the contaminant is limited by the flux-weighted injection mode. From a different perspective, we highlight that this graphical tool permits to clearly identify hot spots and hot moments. In this context, it is interesting to see that the area of $\xi_{c_i}(x,t)$ reaching a given predefined threshold at any given time (hot spot) and its corresponding temporal persistence (hot moment) decreases with heterogeneity (σ_Y^2). On the contrary, the flux-weighted injection mode promotes larger hot spots and hot moments.

4.2. Total Increased Lifetime Cancer Risk

4.2.1. Low-Order Moments and Reliability

Additive risk models determine that the ILCR posed by a chemical mixture is the sum of the risk posed by each chemical species in the chemical mixture, equation (4). The total risk low-order moments are shown in Figure 4. Results demonstrate that, when the toxicity of intermediate products is larger than that of the parent species, the mean total risk can increase to a maximum (R_c) at a critical position (x_c). The area with elevated risk surrounding this critical position is denoted as a *hot spot*. Between the contamination area ($x=x_{inj}$) and the critical position ($x=x_c$) the rate of risk generation due to the formation of toxic intermediate products exceeds the rate of risk reduction due to self-purification (natural attenuation). Eventually, the total risk decreases to near zero at larger distances meaning that the aquifer can remediate itself by natural attenuation.

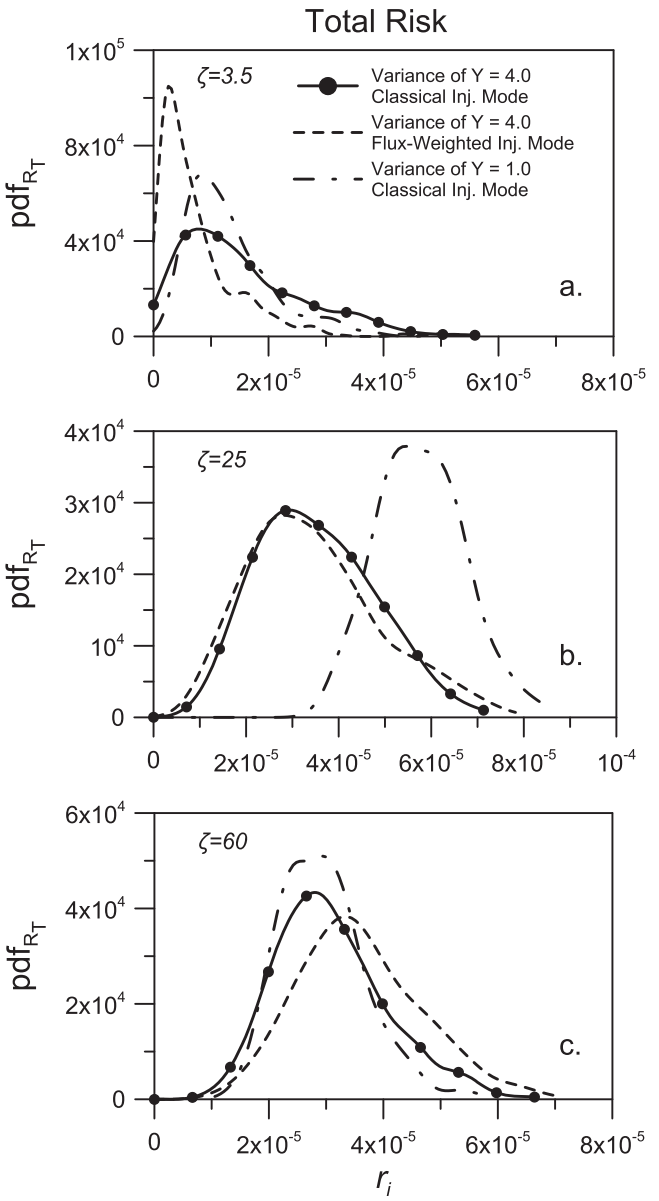

Figure 6. Probability density functions (*pdfs*) of the total increased lifetime cancer risk obtained at different control planes with normalized distance $\zeta = 3.5$, 25, and 60.

Results also indicate that careful attention should be paid to the risk metrics employed during the management of chemical mixtures at a hazardous waste site. A completely different depiction of the critical hot spot can be obtained by using the probability of exceedance of MCLs. For instance, section 4.1 shows that the largest probability of exceedance of the MCL associated with the parent species PCE is situated nearby the source zone and far from the critical position x_c.

The critical position x_c depends on the joint effect of PCE and degradation products on the total risk. The relative contribution of each species is depicted in Figure 5. The individual risk posed by PCE and TCE is 2 orders of magnitude lower than DCE and VC. Consequently, the contribution of PCE and TCE to the total risk is negligible and the total mean risk is mainly controlled by DCE and VC. Figure 5b displays the uncertainty in risk predictions. Interestingly, the coefficient of variation (CV_{R_T}) shows a strong inverse correlation with its mean value. Thus, low risk values nearby the source zone have large uncertainties and high risk values close to the critical position are the most reliable.

The probability to exceed a mandated risk threshold $\xi_{R_T}(\mathbf{x})$ follows the total mean risk behavior (Figure 5c) but exhibits a larger area, centered at the critical position, within which the risk persists beyond a specified threshold. That is to say that the area required to accomplish an apparent decontamination can be large in practical situations. Moreover, even though the mean risk at the source zone is close to the critical threshold ($R^* = 10^{-5}$), we note that the probability to exceed R^* is still substantial. An effect that seems attributable to the high uncertainty attained in this region.

Heterogeneity favors the development of preferential channels through which contaminants can rapidly be transported from the source zone to further away distances [*Gomez-Hernandez and Wen*, 1998; *Zinn and Harvey*, 2003]. Consequently, Figure 4a shows that the critical distance increases with σ_Y^2. At the same time, the maximum risk value diminishes with σ_Y^2 due to the combination of enhanced macrodispersive effects and the subsequent dilution of concentrations at control planes. Large σ_Y^2 not only diminish the maximum total risk attained at the critical position but also spreads the risk over a wider area (Figure 4a). The CV_{R_T} analysis shows also a significant sensitivity to the degree of heterogeneity (Figure 4b), especially, close to the source and at the hot spot where the uncertainty in risk predictions increases with σ_Y^2. Finally, heterogeneity causes the persistence of large ξ_{R_T} values over a wider area (Figure 4c).

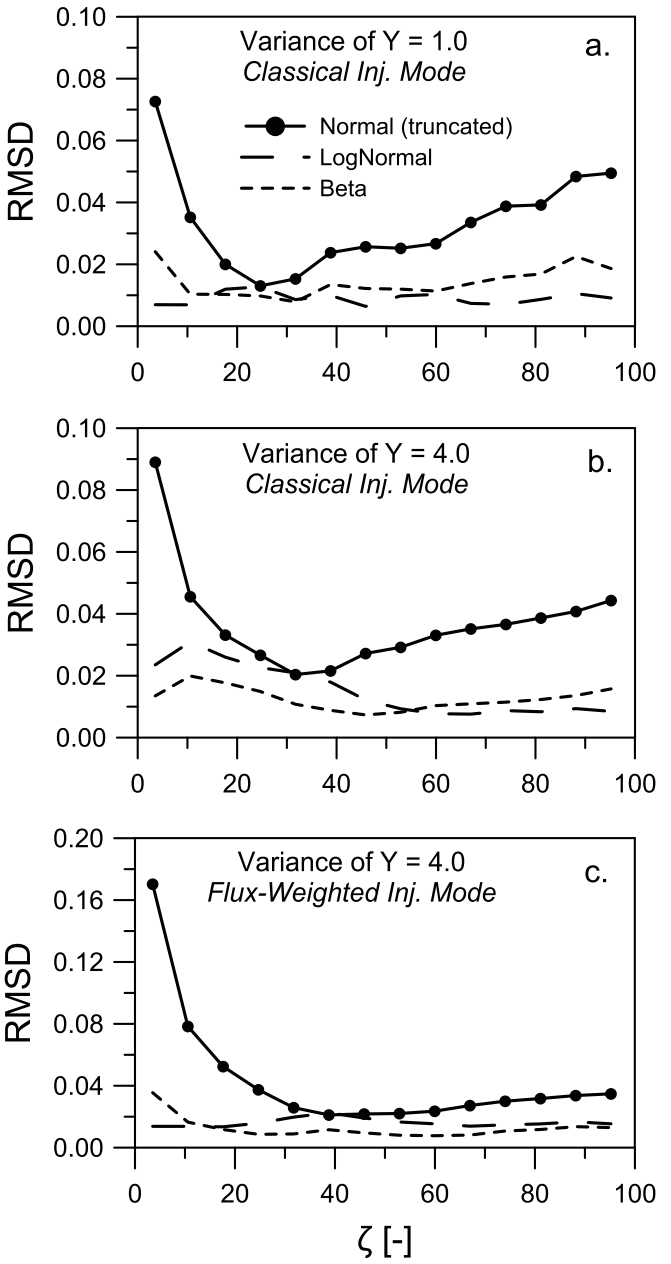

Figure 7. Root-mean-square deviation between theoretical Beta, Lognormal, and (truncated) Normal distributions, and the total increased lifetime cancer risk obtained from Monte Carlo simulations as a function of the normalized travel distance.

A flux-weighted injection mode (particles injected proportional to local fluxes) initially concentrates more mass in preferential flow channels [*Vanderborght et al.*, 1998]. This effect precludes the initial mixing of the contaminant nearby the injection location, causing an increase in the maximum total mean risk and the critical distance (see Figure 4a). As a result, the probability to exceed a mandated risk threshold is shifted away from the source zone during a flux-weighted injection (Figure 4c).

4.2.2. Probability Density Functions

The total risk-*pdf*s are shown in Figure 6 as a function of σ_Y^2 and the injection mode for three different normalized traveled distances ($\zeta = 3.5$, 25.0, and 60.0). Results demonstrate that biodegradation can effectively modify the form of the risk-*pdf*s. These *pdf*s are highly asymmetric, positively skewed nearby the source zone ($\zeta = 3.5$ in Figure 6a) due to the high probability of occurrence of the less toxic compounds in this region. The total risk-*pdf*s seem to approach a Gaussian-like behavior with travel distance (Figures 6b and 6c). The effect of heterogeneity on the total risk-*pdf*s is also shown in Figure 6. Close to the source zone ($\zeta = 3.5$), a large σ_Y^2 yields residual but persistent probabilities of high risk.

The flux-weighted injection mode favors the production of degradation products at larger travel distances. Consequently, knowing that the total risk behavior is mostly controlled by the most toxic species DCE and VC, a flux-weighted injection leads to positively skewed distributions of risk with a peak centered toward smaller risk values (Figure 6a).

The total risk-*pdf*s also displays the probability of having negligible risk. This effect depends on the production and the consumption time of the species involved and the travel time needed to reach a certain distance. Thus, negligible risk is highly probable at short traveled distances (Figure 6a) due to the late production of the most toxic species, VC. Heterogeneity affects the probability of negligible risk. The formation of preferential channels favored by large σ_Y^2 and flux-weighted injections increases the probability of negligible risk by promoting the rapid migration of products to far away distances.

Describing the risk-*pdf*s by their closest probability density function model provides useful information for a future characterization of risk in real applications. To study this, the sample total risk-*pdf*s (Figure 6) were

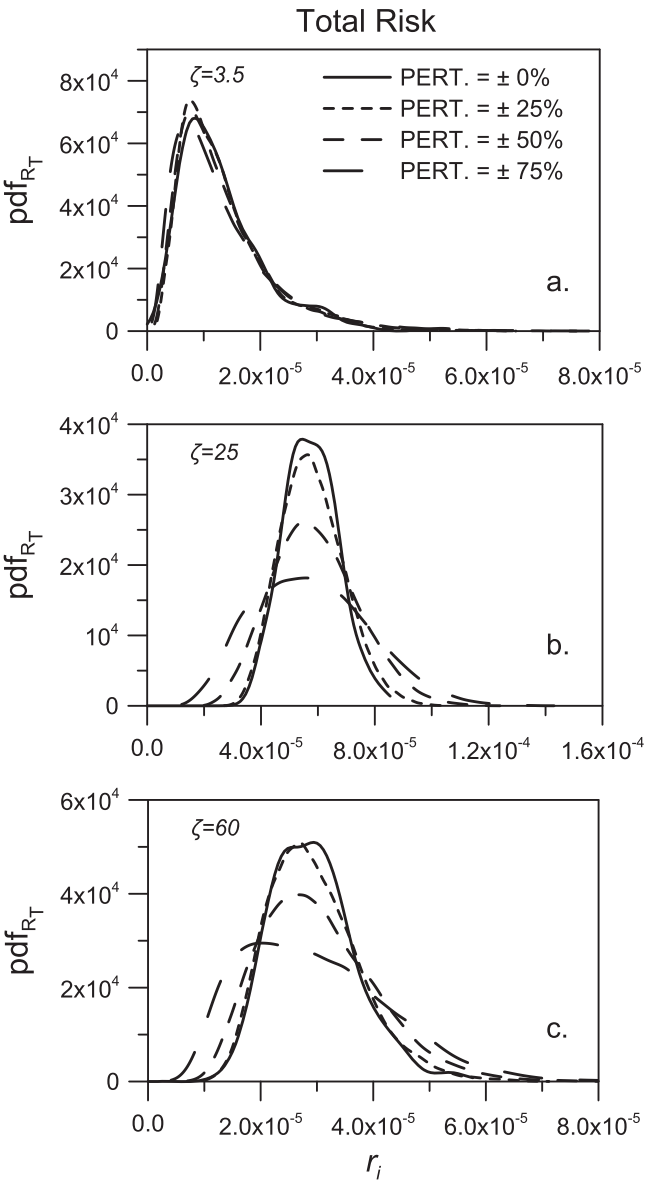

Figure 8. Probability density functions (*pdfs*) of the total increased lifetime cancer risk considering different degrees of perturbations around the mean of the species-specific cancer potency factors for $\sigma_Y^2 = 1.0$ and normalized distances $\zeta = 3.5$, 25, and 60.

fitted to different theoretical distribution functions honoring the mean and the variance of the ensemble. The Kolmogorov-Smirnov (K-S) test at a 95% confidence level indicates that the risk-*pdfs* obtained in high-risk areas (hot spots) (Figure 6b) do not significantly deviate from a Gaussian distribution. In other areas, the K-S tests were only satisfied for the lognormal and beta distribution. This seems to be in agreement with results typically reported in the literature for the concentration *pdfs* [e.g., *Bellin et al.*, 1994; *Rubin et al.*, 1994; *Bellin and Tonina*, 2007; *Sanchez-Vila et al.*, 2008; *Dentz*, 2012; *de Barros and Fiori*, 2014]. The root-mean-square-deviations (RMSD) of the best fit between the theoretical distributions (truncated normal, lognormal, and beta) and the sample total risk-*pdfs* are also shown in Figure 7. The Gaussian-like behavior of the risk distribution obtained in hot spots is here confirmed. In regions with limited or advanced degradation products production (at short and large travel distances, i.e., $\zeta \lesssim 20$ and $\zeta \gtrsim 50$), the risk distribution seems to follow a lognormal or beta distribution. The different scenarios show consistent results (Figures 7a–7c).

The impact that the uncertainty in toxicological parameters has on total risk predictions was also investigated. To consider this, a random perturbation of the previously used cancer potency factors was introduced into equation (1). The perturbed cancer potency factors were described by pseudorandom numbers taken from a uniform distribution supported on a bounded interval defined by $\mu(1 \pm 25\%)$, $\mu(1 \pm 50\%)$, and $\mu(1 \pm 75\%)$, where μ denotes the previously defined CPFs. Figure 8 shows the results obtained for $\sigma_Y^2 = 1$. When the mass of the chemical products controlling the total risk is small, i.e., nearby the source zone ($\zeta = 3.5$), the uncertainty in physiological parameters do not substantially affect the risk-*pdfs* predictions (Figure 8a). In this case, the uncertainty in the hydraulic conductivity is the controlling factor. However, in areas where the mass of the products DCE and VC is abundant ($\zeta = 25.0$ and 60.0), a perturbation of the CPFs will gradually deteriorate the Gaussian-like behavior observed in the risk-*pdfs* (Figures 8b and 8c). This result agrees with the conclusions of *de Barros and Rubin* [2008].

5. The Toxicology-Based Damkhöhler Number

Results have demonstrated that, when the toxicity of intermediate products is larger than that of the parent species, the mean total risk can reach a maximum value (R_c) at a critical position (x_c). At this critical position,

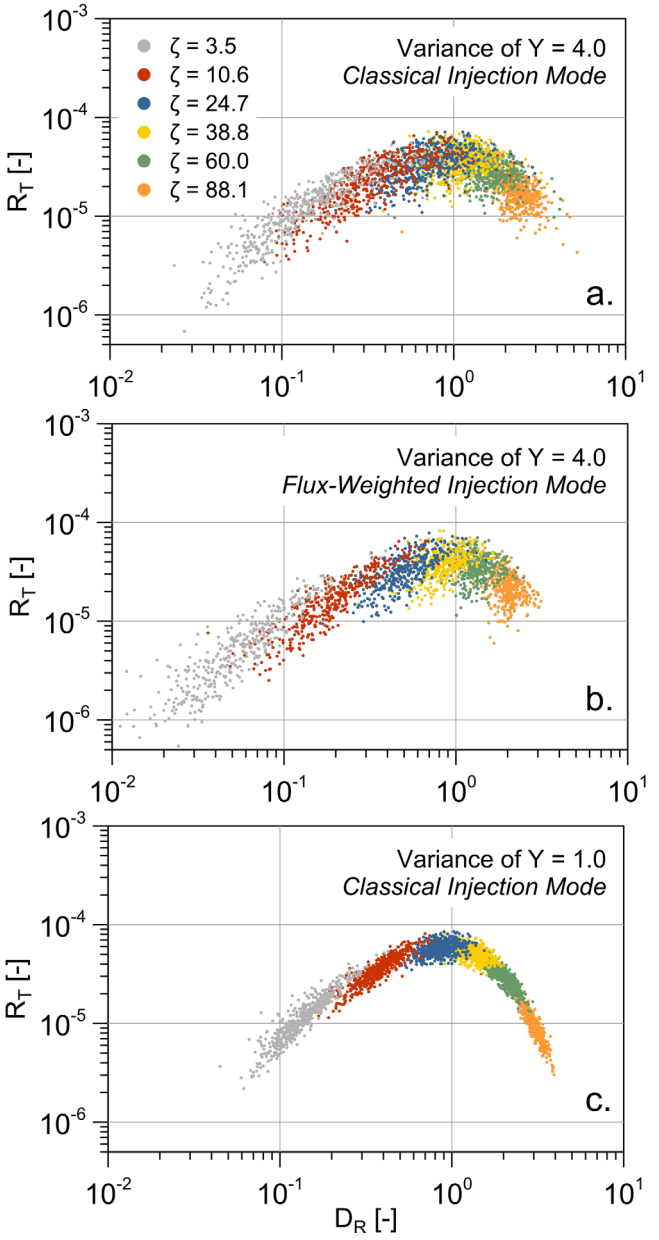

Figure 9. Relationship between the total increased lifetime cancer risk and the toxicological-based Damköhler number obtained for each simulation and scenario at selected control planes.

the rate of risk generation due to the formation of toxic intermediate products is equal to the rate of risk reduction due to self-purification (natural attenuation). Based on this, it is useful to define a dimensionless number D_R to relate the distance of a sensitive location ($d=x-x_{inj}$) to the corresponding critical distance ($d_c=x_c-x_{inj}$),

$$D_R=\frac{d}{d_c}. \tag{14}$$

The sensitive location will be situated downgradient or upgradient from the critical position depending on D_R, i.e., $D_R > 1$ will indicate that the sensitive location is downgradient and vice versa. Knowing this dimensionless number, the relative distance between the sensitive location and the critical position can be estimated by:

$$\ell=\left|\frac{d-d_c}{d_c}\right|=|D_R-1|. \tag{15}$$

The estimation of D_R in the field requires several considerations. The distance to the sensitive location d is known by construction but the location of the hot spot (d_c) is largely uncertain. Let us express this critical distance as $d_c=v_a\bar{t}_c$, where $\bar{t}_c$ is the mean arrival time needed for a nonreactive solute to reach the critical distance, and v_a is the apparent velocity of groundwater. An approximate solution of $\bar{t}_c$ can be determined analytically by noticing that the total mass of a given species is closely related to the maximum running averaged flux-concentration. The derivation is provided in the appendix. Because $\bar{t}_c$, which is referred to as the critical time, can be analytically determined from toxicological and chemical properties, D_R can be seen as a toxicology-based Damköhler number. However, v_a depends mostly on the spatial variability of the hydraulic conductivity field and is susceptible to large uncertainties. This uncertainty will propagate to D_R. The following section analyzes how this uncertainty can affect the total risk predictions.

To illustrate the importance of the toxicology-based dimensionless number, we estimated D_R from (14) for each realization and x-control plane. The critical time $\bar{t}_c$ was estimated from the analytical solution provided in Appendix A, i.e., from equation (A15). For each realization, we also simulated the transport of a nonreactive species with an instantaneous injection. The resulting breakthrough curve is denoted as c^{δ}. From this, v_a at a given x-control plane was calculated as $v_a=d/\bar{t}(x)$, where $\bar{t}(x)$ is the mean arrival time determined from:

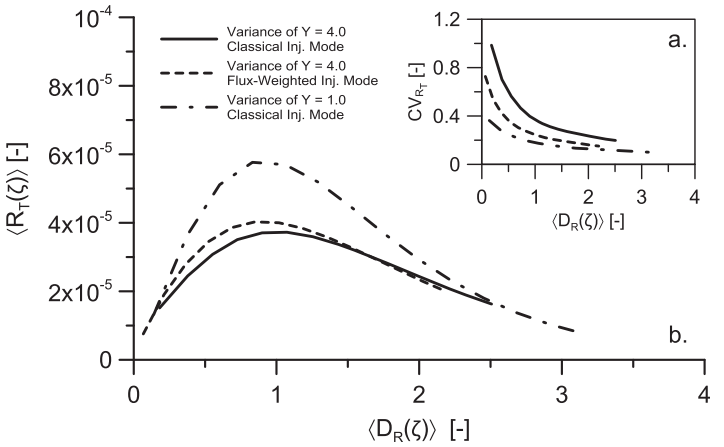

Figure 10. (a) Coefficient of variation and (b) mean of the total increased lifetime cancer risk as a function of the mean toxicological-based Damköhler number obtained at each control plane for all scenarios.

$$\bar{t}(x)=\frac{\int_0^\infty tc^\delta(t;x)dt}{\int_0^\infty c^\delta(t;x)dt}. \quad (16)$$

Figure 9 shows the ensemble of the total risk R_T as a function of D_R. Here colors are used to distinguish data from different selected control planes. Results show that the maximum total risk satisfies that $D_R = 1$ in all cases. Interestingly, the total risk is positively correlated with D_R when $D_R < 1$ and negatively correlated when $D_R > 1$. That is to say that between the contamination area and the critical distance the total risk increases with ℓ, whereas beyond the critical distance the total risk decreases with ℓ. Essentially, the first regime is controlled by the production of highly toxic intermediate species and the second regime is controlled by the self-purification capacity of the aquifer due to natural attenuation.

The relationship between total risk and the toxicology-based Damköhler number as a function of σ_Y^2 and injection mode is better seen by presenting the ensemble average of the two quantities over all realizations at each control plane (Figure 10). In this context, the degree of heterogeneity σ_Y^2 seems to dictate the intensity of R_T for a given D_R. The intensity decreases with increasing σ_Y^2, suggesting a tendency to dilute the hazard. The effect of the injection mode is seen moderate in this case.

6. Impact of Connectivity

Low-order moments of a random field (mean, variance, and covariance function) do not provide sufficient information on the structure of preferential channels, which mainly control v_a in a given realization. In other words, two realizations with the same low-order moments can reflect substantially different connectivity features and, in turn, apparent velocity estimates [*Gomez-Hernandez and Wen*, 1998].

Different metrics have been used to describe connectivity [*Sanchez-Vila et al*., 1999; *Fernàndez-Garcia et al*., 2002; *Knudby and Carrera*, 2005, 2006; *Trinchero et al*., 2008; *Fernàndez-Garcia et al*., 2010]. In general, *Renard and Allard* [2013] distinguished two types of measures: *Static* connectivity metrics only depend on the spatial distribution of aquifer properties, and *dynamic* connectivity metrics depend on the flow and/or transport response to a given impulse. To analyze the effect of connectivity on risk, this section categorizes risk simulations in terms of a dynamic connectivity metric. The chosen connectivity metric *CI* is defined as the ratio of the effective hydraulic conductivity, K_{eff}, to the geometric mean of K, K_G [*Knudby and Carrera*, 2005],

$$CI=\frac{K_{eff}}{K_G}\approx\frac{1}{t_{50}}\frac{(x_{cp}-x_{inj})\,\phi}{K_G J}, \quad (17)$$

where t_{50} is the arrival time of the 50% of mass. High *CI* values indicate the presence of preferential channels and vice versa. This connectivity metric was estimated for all realization to represent *CI* as a function of the total risk (Figures 11d–11f). For comparison purposes, we also estimated the relationship between *CI* and the individual risk posed by PCE (Figures 11a–11c).

A clear power law relationship is observed for small σ_Y^2 (Figures 11c and 11f). Yet, this relationship is strikingly different for PCE than for chemical mixtures. Even though the individual risk posed by PCE always tends to increase with connectivity, mostly due to a decrease in the travel time and degradation, this is not necessarily true for chemical mixtures. When $D_R < 1$, the total risk decreases with increasing connectivity but the opposite occurs when $D_R > 1$. This indicates that the impact of connectivity on risk predictions

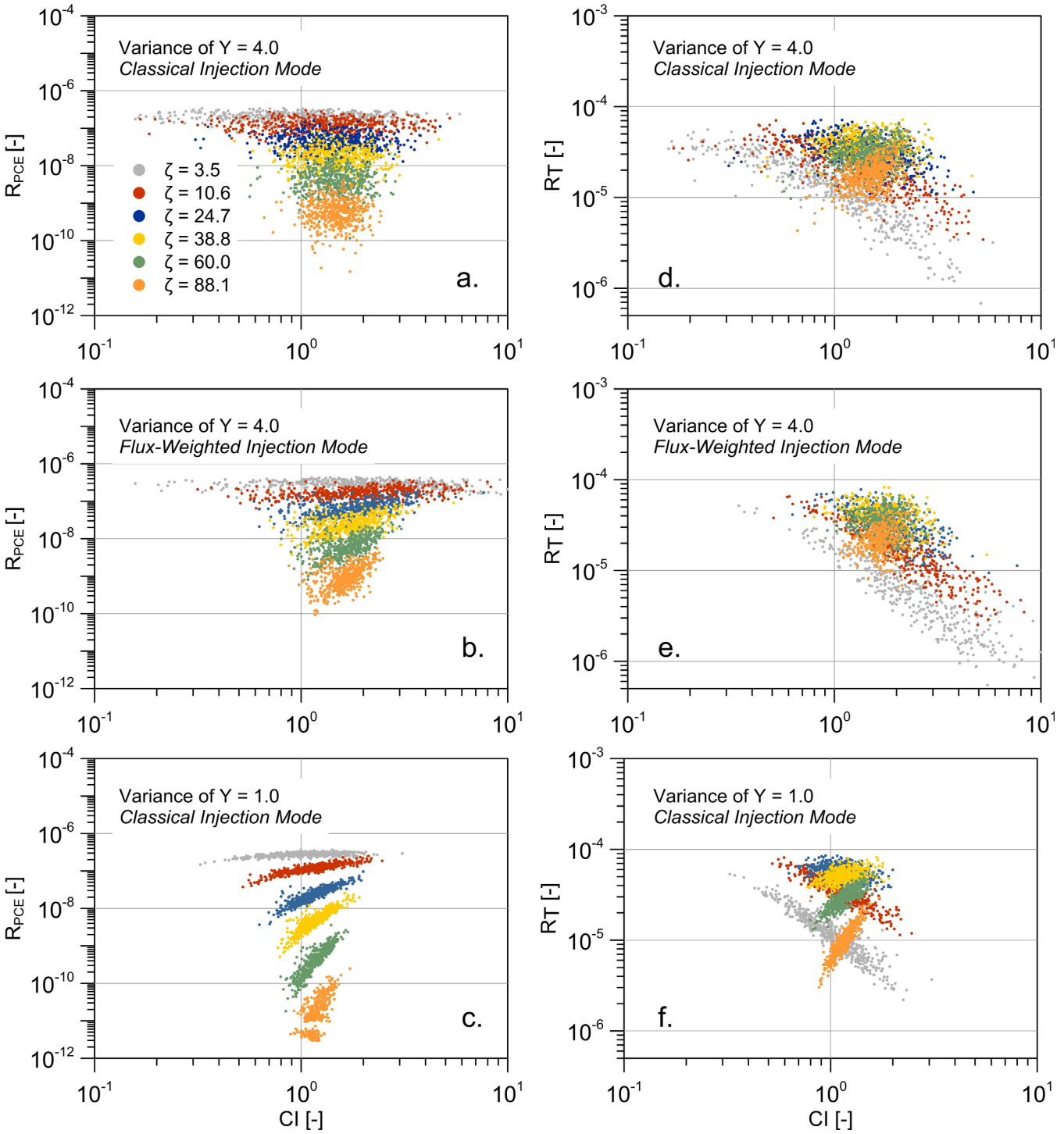

Figure 11. Relationship between the increased lifetime cancer risk related to the exposure to (left) PCE (frames a–c) and to the (right) chemical mixture (frames d–f), and the connectivity indicator obtained for each simulation and scenario at selected control planes.

mostly depends on D_R. When $D_R < 1$, the hot spot is located beyond the sensitive location ($d < d_c$). In this situation, the presence of preferential channels (high *CI* values) will move the hot spot to a farther distance, thereby reducing the total risk. Instead, when $D_R > 1$, the hot spot is located between the source zone and the sensitive location ($d > d_c$). In this case, preferential channels will move the hot spot closer to the sensitive location, thereby increasing the total risk. Figure 12 shows a sketch of these situations.

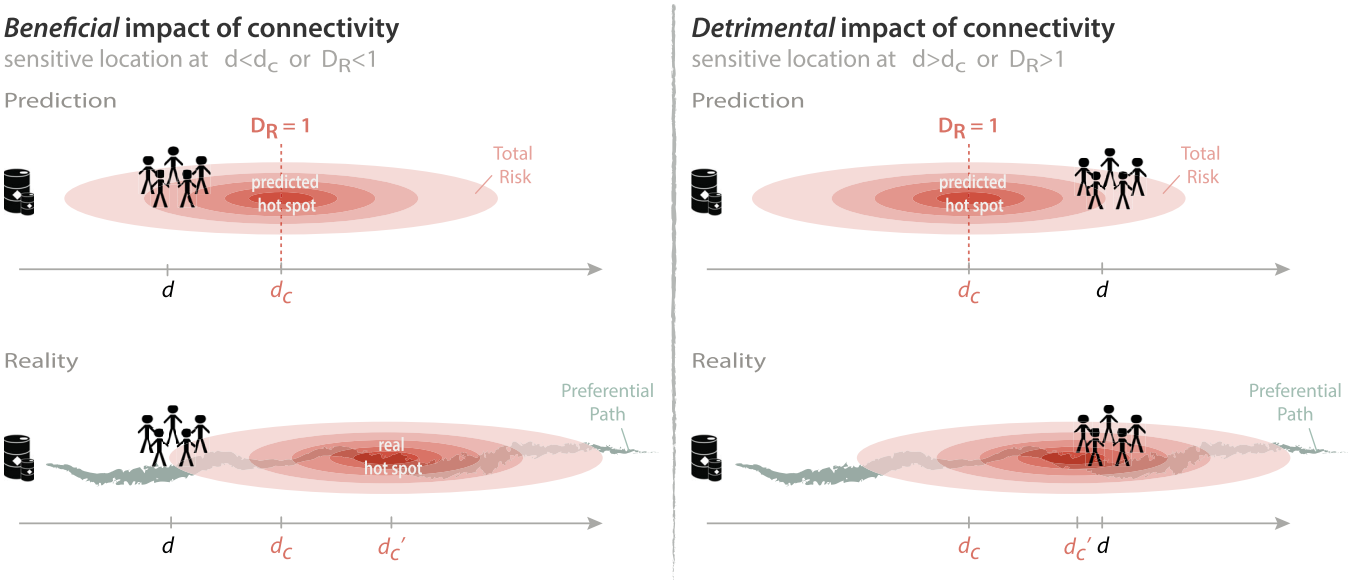

Figure 12. Schematic illustration of the relationship between the toxicological-based Damköhler number (D_R), connectivity (CI), and the total risk (R_T). The red plume represents the spatial distribution of the total risk reaching a maximum at the critical distance d_c. The toxicological-based Damköhler number D_R is equal to 1 at the critical distance. Left figures represent a scenario A in which the exposed population is initially estimated to be located between the source of pollution and the hot spot ($D_R < 1$). Right figures represent a scenario B in which the exposed population is initially estimated to be located beyond the hot spot location ($D_R > 1$). If initial predictions on the critical distance have not considered (or missed) the presence of an existing preferential transport pathway, the real critical distance d_c' will be located at a farther away distance. This will cause a decrease of the total risk in scenario A (beneficial impact of connectivity) but not in scenario B where the total risk increases (detrimental impact of connectivity).

To further explore this, the power law relationship was fitted to the following regression model:

$$R_T = a\,(CI)^b, \tag{18}$$

where $|b|$ expresses the sensitivity of the total risk to connectivity, and the sign of b indicates whether connectivity is beneficial ($b < 0$) or detrimental ($b > 0$) in risk predictions. Results show a strong linear relationship between b and D_R (Figure 13a) with a negative correlation when $D_R < 1$ and a positive correlation when $D_R > 1$. Suppose that one estimates, based on the general properties of an aquifer, that a sensitive

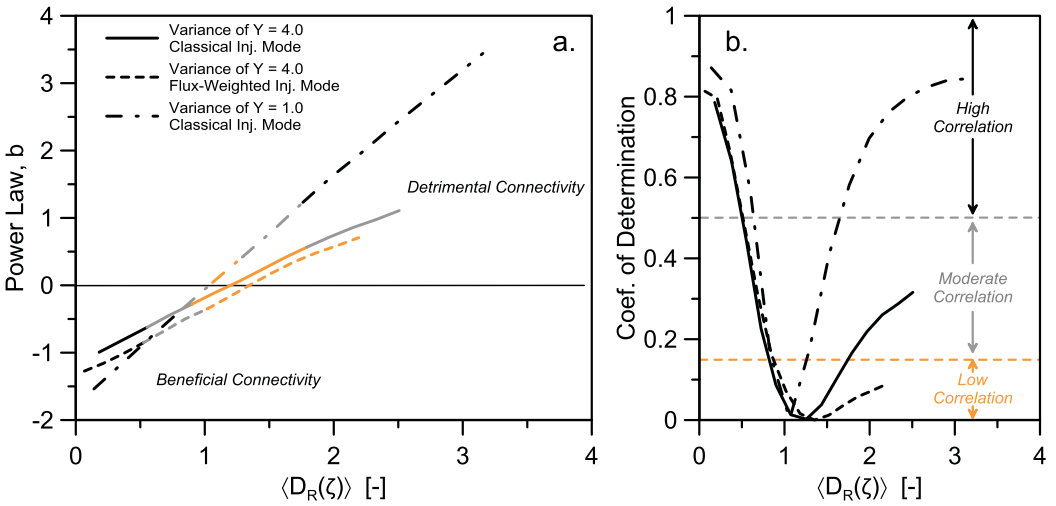

Figure 13. (a) Power regression coefficient β as a function of the mean toxicological-based Damköhler number obtained at each control plane. The line color indicates the degree of correlation between R_T and CI with the following criterion based on the coefficient of determination r^2: black for a high correlation ($r^2 > 0.5$), grey for a moderate correlation ($r^2 < 0.5$), and orange for a low correlation ($r^2 < 0.15$). (b) The coefficient of determination r^2 related to each power regression and color criterion.

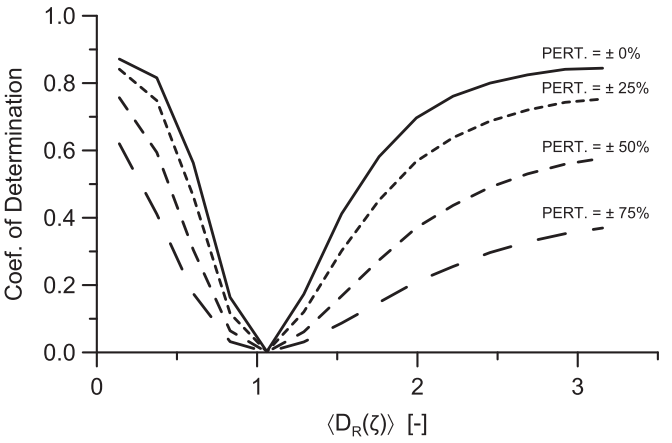

Figure 14. Coefficient of determination r^2 of the regression model $R_T = a(CI)^b$ as a function of the mean toxicological-based Damköhler number for different perturbations of the cancer potency factor.

location (e.g., a populated area) is characterized by $D_R < 1$. In this case, the unnoticed presence of preferential channels at the field site due to the lack of detail characterization will lead to smaller risk predictions than expected. A situation that is conservative in terms of risk. On the contrary, if the sensitive location is characterized by $D_R > 1$, the unnoticed presence of preferential channels can lead to significantly erroneous risk predictions. In this case, one needs to intensify site characterization and monitoring efforts. It is also important to highlight here that the effect of connectivity is expected to be more pronounced in nonmulti-Gaussian fields, where well-connected structures with large permeability values can develop faster solute pathways [*Gomez-Hernandez and Wen*, 1998].

Despite this clear trend, the correlation between *CI* and D_R diminishes close to hot spots ($D_R = 1$) and large σ_Y^2 values (Figure 13c). This is seen for both injection modes without substantially affecting the results. In sum, the unnoticed presence of preferential channels can lead to catastrophic consequences in cases where D_R is large ($d > d_c$) and σ_Y^2 is relatively small. Finally, we note that other sources of uncertainty can also affect this relationship. For instance, the uncertainty in toxicity measures (see section 4.2.2) seems to deteriorate the fit to the regression model without significantly affecting the parameters (Figure 14).

7. Concluding Remarks

We have investigated human health risk of a chemical mixture, formed by the combination of tetrachloroethylene with its daughter products, in a three-dimensional heterogeneous aquifer under uncertainty through a set of Monte Carlo reactive-transport simulations involving a multispecies chemical system. Simulation results have provided a full statistical description of the most common risk metrics (increased lifetime cancer risk and probability of exceedance of MCLs) as well as an examination of the key factors controlling the formation of hot spots (high-risk areas). The following main findings are highlighted:

1. *Uncertainty and Reliability*. The statistical analysis of the increased lifetime cancer risk has demonstrated that low risk values, observed far from the source zone for the parent species and near the source for the degradation products, have typically large uncertainties. Contrarily, high-risk areas are the most reliable. This is in line with previous works that found low reliability at low expected concentrations [*Kapoor and Gelhar*, 1994]. We have also proposed a visualization tool aimed at analyzing the probability of exceedance of MCLs during the temporal and spatial risk management of a contaminated site. Interestingly, results have determined that the area of nonzero probability of MCLs increases with σ_Y^2, owing to the formation of preferential channels and fast travel times, but they take place during a shorter period of time due to an increase dilution of the contaminant in the system. Moreover, a flux-weighted injection mode has led to a decrease in reliability in both space and time by limiting the dilution process while increasing travel times.

2. *Probability Distributions Forms*. Total risk *pdf*s have shown positively skewed asymmetric distributions with a maximum at a relatively low risk value near the source zone. This is especially true for small σ_Y^2 or when a nontrivial flux-weighted injection mode is considered. The emergence of asymmetric distributions may lead to reinterpret the a priori expected risk value and reliability, which is, respectively, overestimated and underestimated. The functional form of the risk-*pdf* is determined to follow a Gaussian-like behavior nearby areas of elevated risk. However, in other areas, the distribution is better characterized by a lognormal or a beta distribution.

3. *Formation of Hot Spots*. Risk analysis of chemical mixtures cannot consider that corresponding hot spots (here defined as areas of elevated risk) are somehow located close to the contaminant source where concentrations are higher. In a chemical mixture, the joint effect of advection, degradation pathways and toxicity dictates the formation of a hot spot. A newly proposed toxicity-weighted Damköhler number D_R has been shown to control the longitudinal distribution of the total risk, which tends to increase with D_R to a maximum at a certain critical position x_c where $D_R = 1$. The time needed for a conservative species to reach this critical distance ($\bar{t}_c$) depends on toxicity and biochemical properties. Approximate analytical solutions of this critical time are provided. These results differ from observation made on more trivial cases, where early arrivals are often seen as the most dangerous cases. On the other hand, the amplitude of the mean total risk is mainly a function of σ_Y^2.
4. *The Role of Connectivity*. The assessment of human health risk based only on low-order statistical moments is shown to provide an incomplete analysis of risk. An additional key factor is shown to be connectivity. Results have illustrated that a hydraulic conductivity field with high connectivity is susceptible to have a beneficial ($D_R < 1$ or $x < x_c$) or a detrimental ($D_R > 1$ or $x > x_c$) effect on risk depending on the proposed toxicity-weighted Damköhler number. If a sensitive area is characterized by $D_R < 1$, the unnoticed presence of a preferential channel due to the lack of detail characterization is shown to lead to smaller risk estimates than expected. A situation that is conservative in terms of risk (overestimation). On the contrary, if the sensitive area is characterized by $D_R > 1$, the unnoticed presence of a preferential channel can have important consequences as it is shown to lead to higher than expected risk estimates. In this case, one needs to intensify site characterization and monitoring efforts.

Appendix A: The Total Risk Critical Time and Distance

A closed-form analytical solution of the critical distance x_c and the critical time t_c at which the total increased lifetime cancer risk (ILCR) reaches a maximum value is derived in this appendix. We start by noticing that since $\bar{c}_i(x)$ only depends on x and the partial differential equations describing contaminant transport constitutes a linear system, the critical distance x_c is independent of the temporal evolution of the source term $c_s(t)$. This term will only affect the intensity of the total risk but not its critical position. Based on this, it is mathematically convenient to solve the critical distance x_c for a Dirac-input source of the form $Q_s c_s(t) = m_0 \delta(t)$, where m_0 is the total initial contaminant mass of PCE at the source zone.

By the definition of the maximum running averaged flux-concentration obtained at the x-control plane we have that:

$$Q_d\, \bar{c}_i(x)\, ED = \int_{t_p - \frac{ED}{2}}^{t_p + \frac{ED}{2}} Q_d\, c_i(t; x)\, dt, \tag{A1}$$

where Q_d is the total flow rate passing through the x-control plane, and t_p is the time where the risk reaches its maximum point. In the limit, when $ED \to \infty$, the integral in the right-hand side of equation (A1) is simply the total mass of species i recovered at the control plane. The exposure duration ED is typically a large number ranging between 30 years (noncarcinogens) and 70 years (for carcinogens). In this situation, this integral can be seen as some proportion α of the total mass. Imagine, for instance, that the concentration profile is Gaussian and ED is about 4 standard deviations, in this case, $\alpha = 95\%$. This reasoning suggests that one can approximate the integral in (A1) by:

$$Q_d\, \bar{c}_i(x)\, ED \approx \alpha\, M_i \left(\frac{d(x)}{v_a} \mathcal{R}_i^e \right), \tag{A2}$$

where $d(x) = x - x_{inj}$ is the distance from the source zone to the x location, and v_a is the apparent velocity of groundwater (defined from the mean arrival time of a conservative species at the x control plane as $v_a = d(x)/\bar{t}(x)$, $\mathcal{R}_i^e$ is the effective retardation factor of the ith species, and M_i is the total mass of species i defined by:

$$M_i(t) = \int_{-\infty}^{\infty} \mathcal{R}_i\, \phi\, C_i(\mathbf{x}, t)\, d\mathbf{x}. \tag{A3}$$

The additivity property of risk states that the total ILCR for a system composed of n_s toxic chemical species is

$$\mathrm{R_T}(x) = \sum_{i=1}^{n_s} \mathrm{R}_i(x). \tag{A4}$$

The human health risk model (section 2.1) relates the ILCR of a given species i to the maximum running averaged flux-concentration $\bar{c}_i$ and the toxicological parameters. For the sake of simplicity, one can simply express that

$$\mathrm{R}_i(x)=\beta_i\,\bar{c}_i(x), \tag{A5}$$

where

$$\beta_i=CPF_i\times\left[\frac{IR}{BW}\right]\frac{ED\times EF}{AT}. \tag{A6}$$

Substituting (A2) and (A5) into (A4) we obtain

$$\mathrm{R}_\mathrm{T}(x)=\frac{\alpha}{Q_d\,ED}\sum_{i=1}^{n_s}\beta_i M_i\left(\frac{d(x)}{v_a}\mathcal{R}_i^e\right). \tag{A7}$$

The critical distance x_c at which the total increased lifetime cancer risk reaches a maximum level is

$$x_c=\arg\max_x\{\mathrm{R}_\mathrm{T}(x)\}, \tag{A8}$$

which can be obtained by setting $\partial R_T/\partial x=0$,

$$\frac{\partial}{\partial x}\sum_{i=1}^{n_s}\beta_i M_i\left(\frac{d(x)}{v_a}\mathcal{R}_i^e\right)=0. \tag{A9}$$

Defining $\bar{t}=d(x)/v_a$, this equation can be rewritten as

$$\frac{\partial}{\partial\bar{t}}\sum_{i=1}^{n_s}\beta_i M_i\left(\bar{t}\mathcal{R}_i^e\right)=0. \tag{A10}$$

Knowing $M_i(t)$, the solution of this implicit equation yields the critical time $\bar{t}_c$ needed for a conservative tracer to reach the critical risk distance. Thus,

$$\bar{t}_c=\arg\max_{\bar{t}}\left\{\sum_{i=1}^{n_s}\beta_i M_i\left(\bar{t}\mathcal{R}_i^e\right)\right\}. \tag{A11}$$

The temporal evolution of the total mass of a given species i can be determined from the mass balance equations of the chemical system, written as:

$$\frac{dM_i(t)}{dt}=\frac{y_i k_{i-1}}{\mathcal{R}_{i-1}}M_{i-1}(t)-\frac{k_i}{\mathcal{R}_i}M_i(t)+m_0\delta(t)\delta_{i1},\ \forall i=1,\ldots,n_s, \tag{A12}$$

where δ_{i1} is the Kronecker delta (only PCE is released from the source zone). This is a system of ordinary differential equations whose solution is

$$\mathbf{M}(t)=m_0 e^{\mathbf{A}(t)}\mathbf{e}_1, \tag{A13}$$

where $\mathbf{M}(t)=[M_1(t),\ldots,M_n(t)]^t$, $\mathbf{e}_1=[1,0,\ldots,0]^t$, and $\mathbf{A}$ is a lower triangular matrix with diagonal elements determined by $A_{ii}=-k_i/\mathcal{R}_i$ and nonzero satellite elements determined by $A_{ii-1}=y_i k_{i-1}/\mathcal{R}_{i-1}$. This matrix $\mathbf{A}$ can be easily decomposed by the eigenvalue method into $\mathbf{A}=\mathbf{SDS}^{-1}$, where $\mathbf{D}$ is a diagonal matrix formed from the eigenvalues of $\mathbf{A}$, and the columns of $\mathbf{S}$ are the corresponding eigenvectors of $\mathbf{A}$. In a similar problem, *Clement* [2001] and *Henri and Fernàndez-Garcia* [2014] showed that these matrices can be written as

$$D_{ii}=-k_i/\mathcal{R}_i,$$

$$S_{ij}=S_{ij}^{-1}=0,\qquad j>i,$$

$$S_{ij}=S_{ij}^{-1}=1,\qquad j=i,$$

$$S_{ij}=\mathcal{R}_i\mathcal{R}_j^{i-j-1}\prod_{m=j}^{i-1}\left(\frac{k_m y_{m+1}}{\mathcal{R}_j k_{m+1}-\mathcal{R}_{m+1}k_j}\right),$$

$$S_{ij}^{-1} = \mathcal{R}_i^{i-j} \prod_{m=j}^{i-1} \left(\frac{-k_m y_{m+1}}{\mathcal{R}_m k_i - \mathcal{R}_i k_m} \right).$$

From this, the mass evolution of each species is written as

$$M_i(t) = m_0 \sum_{j=1}^{n_s} S_{ij} e^{D_{ij} t} S_{j1}^{-1}, \tag{A14}$$

so that the critical time $\bar{t}_c$ is

$$\bar{t}_c = \arg\max_{\bar{t}} \left\{ \sum_{i=1}^{n_s} \sum_{j=1}^{n_s} \beta_i S_{ij} e^{-k_i \bar{t} \mathcal{R}_i^e / \mathcal{R}_j} S_{j1}^{-1} \right\}. \tag{A15}$$

Assuming that the chemical properties are spatially constant, *Henri and Fernàndez-Garcia* [2014] has recently shown that the effective retardation factor associated with a network reaction system is time-dependent properties that depend on the initial conditions of the chemical system. When only PCE is initially present in the aquifer, the effective retardation factors can be estimated from

$$\mathcal{R}_i^e(t) = \frac{M_i(t)}{m_0} \left(\sum_{p,q,r=1}^{n_s} S_{ip} S_{pq}^{-1} \mathcal{R}_q^{-1} S_{qr} S_{r1}^{-1} F_{pr}(t) \right)^{-1}, \tag{A16}$$

where

$$F_{pr}(t) = \begin{cases} \dfrac{\exp(-k_p/\mathcal{R}_p t) - \exp(-k_r/\mathcal{R}_r t)}{t(-k_p/\mathcal{R}_p + k_r/\mathcal{R}_r)}, & \text{if } p \neq r \\ \exp(-k_r/\mathcal{R}_r t), & \text{if } p = r \end{cases}. \tag{A17}$$

We refer to *Henri and Fernàndez-Garcia* [2014] for further details on the effective retardation factor.

Acknowledgments
The authors acknowledge the financial support provided by the Spanish Ministry of Science and Innovation through the SCARCE Consolider-Ingenio 2010 program (reference CSD2009-00065) and project FEAR (CGL2012–38120). The paper provides all the information needed to replicate the results. These data are also freely available from the authors upon request. This work was partially developed when the first author of the article was a visiting scholar at the University of Southern California (CA, USA).

References

Andričević, R., and V. Cvetković (1996), Evaluation of risk from contaminants migrating by groundwater, *Water Resour. Res.*, *32*(3), 611–621, doi:10.1029/95WR03530.
Andričević, R., V. Srzic, and H. Gotovac (2012), Risk characterization for toxic chemicals transported in aquifers, *Adv. Water Resour.*, *36*, 86–97.
Atchley, A. L., R. M. Maxwell, and A. K. Navarre-Sitchler (2013), Human health risk assessment of CO_2 leakage into overlying aquifers using a stochastic, geochemical reactive transport approach, *Environ. Sci. Technol.*, *47*(11), 5954–5962, doi:10.1021/es400316c.
Atchley, A. L., R. M. Maxwell, and A. K. Navarre-Sitchler (2014), Using streamlines to simulate stochastic reactive transport in heterogeneous aquifers: Kinetic metal release and transport in {CO_2} impacted drinking water aquifers, *Adv. Water Resour.*, *52*, 93–106.
Bellin, A., and D. Tonina (2007), Probability density function of non-reactive solute concentration in heterogeneous porous formations, *J. Contam. Hydrol.*, *94*(1), 109–125.
Bellin, A., Y. Rubin, and A. Rinaldo (1994), Eulerian-Lagrangian approach for modeling of flow and transport in heterogeneous geological formations, *Water Resour. Res.*, *30*(11), 2913–2924.
Benekos, I. D., C. A. Shoemaker, and J. R. Stedinger (2007), Probabilistic risk and uncertainty analysis for bioremediation of four chlorinated ethenes in groundwater, *Stochastic Environ. Res. Risk Assess.*, *21*(4), 375–390, doi:10.1007/s00477-006-0071-4.
Bianchi, M., C. Zheng, C. Wilson, G. R. Tick, G. Liu, and S. M. Gorelick (2011), Spatial connectivity in a highly heterogeneous aquifer: From cores to preferential flow paths, *Water Resour. Res.*, *47*, W05524, doi:10.1029/2009WR008966.
Boso, F., A. Bellin, and M. Dumbser (2012), Numerical simulations of solute transport in highly heterogeneous formations: A comparison of alternative numerical schemes, *Adv. Water Resour.*, *52*, 178–189.
Burnell, D. K., J. W. Mercer, and C. R. Faust (2014), Stochastic modeling analysis of sequential first-order degradation reactions and non-Fickian transport in steady state plumes, *Water Resour. Res.*, *50*, 1260–1287, doi:10.1002/2013WR013814.
Clement, T. P. (2001), Generalized solution to multispecies transport equations coupled with a first-order reaction network, *Water Resour. Res.*, *37*(1), 157–163.
Cunningham, J. A., and I. Mendoza-Sanchez (2006), Equivalence of two models for biodegradation during contaminant transport in groundwater, *Water Resour. Res.*, *42*, W02416, doi:10.1029/2005WR004205.
Cvetković, V., and S. Molin (2012), Combining numerical simulations with time-domain random walk for pathogen risk assessment in groundwater, *Adv. Water Res.*, *36*, 98–107, doi:10.1016/j.advwatres.2011.06.008.
de Barros, F. P. J., and A. Fiori (2014), First-order based cumulative distribution function for solute concentration in heterogeneous aquifers: Theoretical analysis and implications for human health risk assessment, *Water Resour. Res.*, *50*, 4018–4037, doi:10.1002/2013WR015024.
de Barros, F. P. J., and Y. Rubin (2008), A risk-driven approach for subsurface site characterization, *Water Resour. Res.*, *44*, W01414, doi:10.1029/2007WR006081.
de Barros, F. P. J., Y. Rubin, and R. M. Maxwell (2009), The concept of comparative information yield curves and its application to risk-based site characterization, *Water Resour. Res.*, *45*, W06401, doi:10.1029/2008WR007324.
Dentz, M. (2012), Concentration statistics for transport in heterogeneous media due to stochastic fluctuations of the center of mass velocity, *Adv. Water Resour.*, *36*, 11–22, doi:10.1016/j.advwatres.2011.04.005.

Dilley, M., R. S. Chen, U. Deichmann, A. L. Lerner-Lam, M. Arnold, J. Agwe, P. Buys, O. Kjevstad, B. Lyon, and G. Yetman (2005), *Natural Disaster Hotspots: A Global Risk Analysis, Disaster Risk Manage. Ser.*, vol. 5, World Bank Publ. 7376, World Bank, Washington, D. C.

Fay, R. M., and M. M. Mumtaz (1996), Development of a priority list of chemical mixtures occurring at 1188 hazardous waste sites, using the HazDat database, *Food Chem. Toxicol.*, *34*(11–12), 1163–1165.

Fernàndez-Garcia, D., X. Sanchez-Vila, and T. H. Illangasekare (2002), Convergent-flow tracer tests in heterogeneous media: Combined experimental-numerical analysis for determination of equivalent transport parameters, *J. Contam. Hydrol.*, *57*(1–2), 129–145.

Fernàndez-Garcia, D., T. H. Illangasekare, and H. Rajaram (2005), Differences in the scale-dependence of dispersivity estimated from temporal and spatial moments in chemically and physically heterogeneous porous media, *Adv. Water Res.*, *28*(7), 745–759.

Fernàndez-Garcia, D., P. Trinchero, and X. Sanchez-Vila (2010), Conditional stochastic mapping of transport connectivity, *Water Resour. Res.*, *46*, W10515, doi:10.1029/2009WR008533.

Fernàndez-Garcia, D., D. Bolster, X. Sanchez-Vila, and D. M. Tartakovsky (2012), A Bayesian approach to integrate temporal data into probabilistic risk analysis of monitored NAPL remediation, *Adv. Resour. Res.*, *43*, 108–120.

Fiori, A., and I. Jankovic (2012), On preferential flow, channeling and connectivity in heterogeneous porous formations, *Math. Geosci.*, *44*(2), 133–145.

Fure, A. D., J. W. Jawitz, and M. D. Annable (2006), DNAPL source depletion: Linking architecture and flux response, *J. Contam. Hydrol.*, *85*, 118–140.

Gelhar, L. W., C. Welty, and K. Rehfeldt (1992), A critical review of data on field-scale dispersion aquifers, *Water Resour. Res.*, *28*(7), 1955–1974.

Gomez-Hernandez, J. J., and X. Wen (1998), To be or not to be multi-Gaussian? A reflection on stochastic hydrogeology, *Adv. Water Res.*, *21*(1), 47–61.

Harbaugh, A., E. Benta, M. Hill, and M. McDonald (2000), MODFLOW 2000 the US Geological Survey Modular ground-water model-user guide to modularization concepts and the ground-water flow process, *U.S. Geol. Surv. Open File Rep., 00–92*, 121 pp.

Henri, C. V., and D. Fernàndez-Garcia (2014), Towards efficiency in 3D heterogeneous multispecies reactive transport modelling: A particle-tracking solution for first-order decay networks, *Water Resour. Res.*, *50*, 7206–7230, doi:10.1002/2013WR014956.

Jain, M. K., and C. S. Criddle (1995), Metabolism and cometabolism of halogenated C-1 and C-2 hydrocarbon, in *Biotransformations: Microbial Degradation of Health Risk Compounds*, edited by V. P. Singh, pp. 65–112, Elsevier Sci., N. Y.

James, B. R., and S. M. Gorelick (1994), When enough is enough: The worth of monitoring data in aquifer remediation design, *Water Resour. Res.*, *30*(12), 3499–3513, doi:10.1029/94WR01972.

Janković, I., and A. Fiori (2010), Analysis of the impact of injection mode in transport through strongly heterogeneous aquifers, *Adv. Water Resour.*, *33*(10), 1199–1205, doi:10.1016/j.advwatres.2010.05.006.

Kapoor, V., and L. W. Gelhar (1994), Transport in three-dimensionally heterogeneous aquifers: 1. Dynamics of concentration fluctuations, *Water Resour. Res.*, *30*(6), 1775–1788.

Kitanidis, P. K., and P. L. McCarty (2012), *Delivery and Mixing in the Subsurface: Processes and Design Principles for In Situ Remediation*, vol. 4, Springer, N. Y.

Knudby, C., and J. S. Carrera (2005), On the relationship between indicators of geostatistical, flow and transport connectivity, *Adv. Water Resour.*, *28*(4), 405–421.

Knudby, C., and J. Carrera (2006), On the use of apparent hydraulic diffusivity as an indicator of connectivity, *J. Hydrol.*, *329*(3–4), 377–389.

LeBlanc, D. R., S. P. Garabedian, K. M. Hess, L. W. Gelhar, R. D. Quadri, K. G. Stollenwerk, and W. W. Wood (1991), Large-scale natural gradient tracer test in sand and gravel, Cape Cod, Massachusetts: 1. Experimental design and observed tracer movement, *Water Resour. Res.*, *27*(5), 895–910.

Lu, C., P. L. Bjerg, F. Zhang, and M. M. Broholm (2011), Sorption of chlorinated solvents and degradation products on natural clayey tills, *Chemosphere*, *83*(11), 1467–1474.

MacDonald, J. A. (2000), Evaluating natural attenuation for groundwater cleanup, *Environ. Sci. Technol.*, *34*(15), 346–353.

Mackay, D. M., D. L. Freyberg, P. V. Roberts, and J. A. Cherry (1986), A natural gradient experiment on solute transport in a sand aquifer: 1. Approach and overview of plume movement, *Water Resour. Res.*, *22*(13), 2017–2029.

Maxwell, R. M., and W. E. Kastenberg (1999), Stochastic environmental risk analysis: An integrated methodology for predicting cancer risk from contaminated groundwater, *Stochastic Environ. Res. Risk Assess.*, *13*(1–2), 27–47, doi:10.1007/s004770050030.

Maxwell, R. M., W. E. Kastenberg, and Y. Rubin (1999), A methodology to integrate site characterization information into groundwater-driven health risk assessment, *Water Resour. Res.*, *35*(9), 2841–2855.

Maxwell, R. M., S. F. Carle, and A. F. B. Tompson (2007), Contamination, risk, and heterogeneity: On the effectiveness of aquifer remediation, *Environ. Geol.*, *54*(8), 1771–1786, doi:10.1007/s00254-007-0955-8.

Parker, J. C., and E. Park (2004), Modeling field-scale dense nonaqueous phase liquid dissolution kinetics in heterogeneous aquifers, *Water Resour. Res.*, *40*, W05109, doi:10.1029/2003WR002807.

Parker, J. C., and M. T. Van Genuchten (1984), Flux-averaged and volume-averaged concentrations in continuum approaches to solute transport, *Water Resour. Res.*, *20*(7), 866–872, doi:10.1029/WR020i007p00866.

Rao, P. S. C., J. W. Jawitz, C. G. Enfield, R. Falta, M. D. Annabel, and A. L. Wood (2001), *Technology Integration for Contaminated Site Remediation: Cleanup Goals and Performance Metrics*, pp. 410–412, Ground Water Qual., Sheffield, U. K.

Renard, P., and D. Allard (2013), Connectivity metrics for subsurface flow and transport, *Adv. Water Resour.*, *51*, 168–196.

Roberts, P. V., M. N. Goltz, and D. M. Mackay (1986), A natural gradient experiment on solute transport in a sand aquifer: 3. Retardation estimates and mass balances for organic solutes, *Water Resour Res.*, *22*(13), 2047–2058.

Rodak, C., and S. Silliman (2012), Probabilistic risk analysis and fault trees: Initial discussion of application to identification of risk at a well-head, *Adv. Water Resour.*, *36*, 133–45.

Rubin, Y. (2003), *Applied Stochastic Hydrogeology*, Oxford Univ. Press, Oxford, U. K.

Rubin, Y., A. Bellin, and M. Cushey (1994), Modeling of transport in ground water for environmental risk assessment, *Stochastic Hydrol. Hydraul.*, *8*(1), 57–78, doi:10.1007/BF01581390.

Salamon, P., D. Fernàndez-Garcia, and J. J. Gómez-Hernández (2006), A review and numerical assessment of the random walk particle tracking method, *J. Contam. Hydrol.*, *87*(3–4), 277–305.

Sanchez-Vila, X., P. M. Meier, and J. Carrera (1999), Pumping tests in heterogeneous aquifers: An analytical study of what can be obtained from their interpretation using Jacob's method, *Water Resour. Res.*, *35*(4), 943–952.

Sanchez-Vila, X., A. Guadagnini, and D. Fernàndez-Garcia (2008), Conditional probability density functions of concentrations for mixing-controlled reactive transport in heterogeneous aquifers, *Math. Geosci.*, *41*(3), 323–351.

Siirila, E. R., and R. M. Maxwell (2012), Evaluating effective reaction rates of kinetically driven solutes in large-scale, statistically anisotropic media: Human health risk implications, *Water Resour. Res.*, *48*, W04527, doi:10.1029/2011WR011516.

Siirila, E. R., A. K. Navarre-Sitchler, R. M. Maxwell, and J. E. McCray (2014), A quantitative methodology to assess the risks to human health from CO_2 leakage into groundwater, *Adv. Water Resour.*, *36*, 146–164.

Skeen, R. S., J. Gao, and B. S. Hooker (1995), Kinetics of chlorinated ethylene dehalogenation under methanogenic conditions, *Biotechnol. Bioeng.*, *48*, 659–666.

Smalley, J. B., B. S. Minsker, and D. E. Goldberg (2000), Risk-based in situ bioremediation design using a noisy genetic algorithm, *Water Resour. Res.*, *36*(10), 3043–3052.

Soga, K., J. Page, and T. Illangasekare (2004), A review of NAPL source zone remediation efficiency and the mass flux approach, *J. Hazard. Mater.*, *110*(13), 13–27.

Speek, A. J. (1981), Lifespan oral toxicity study of vinyl chloride in rats, *Food Cosmetic Toxicol.*, *19*(3), 317–333.

Tartakovsky, D. M. (2007), Probabilistic risk analysis in subsurface hydrology, *Geophys. Res. Lett.*, *34*, L05404, doi:10.1029/2007GL029245.

Trinchero, P., X. Sanchez-Vila, and D. Fernàndez-Garcia (2008), Point-to-point connectivity, an abstract concept or a key issue for risk assessment studies?, *Adv. Water Resour.*, *31*, 1742–1753.

U.S. Environmental Protection Agency (1989), Risk assessment guidance for superfund, Volume 1: Human health manual (Part A), *Rep. EPA/540/1–89/002*.

U.S. Environmental Protection Agency (1997), *Health Effects Assessment Summary Tables*, FY1997 Update, Environ. Criteria and Assess. Off., Off. of Health and Environ. Assess., Off. of Res. and Dev., Cincinnati, Ohio.

U.S. Environmental Protection Agency (1999), *Anaerobic Biodegradation Rates of Organic Chemicals in Groundwater: A Summary of Field and Laboratory Studies*, Off. of Solid Waste, Washington, D. C.

U.S. Environmental Protection Agency (2000), Supplementary guidance for conducting health risk assessment of chemical mixtures, *Rep. EP A/630/R-00/002*, Washington, D. C.

Vanderborght, J., D. Mallants, and J. Feyen (1998), Solute transport in a heterogeneous soil for boundary and initial conditions: Evaluation of first-order approximations, *Water Resour. Res.*, *34*(12), 3255–3270.

Zinn, B., and C. F. Harvey (2003), When good statistical models of aquifer heterogeneity go bad: A comparison of flow, dispersion, and mass transfer in connected and multivariate Gaussian hydraulic conductivity fields, *Water Resour. Res.*, *39*(3), 1051, doi:10.1029/2001WR001146.